Journal of Alloys and Compounds 876 (2021) 160105

Contents lists available at ScienceDirect

Journal of Alloys and Compounds

journal homepage: www.elsevier.com/locate/jalcom

A systematic study on luminescence characterization of lanthanide-doped BeO ceramic dosimeters

V. Altunal[a,*], V. Guckan[a], A. Ozdemir[b], A. Ekicibil[a], F. Karadag[a], I. Yegingil[c], Y. Zydhachevskyy[d], Z. Yegingil[a]

[a] Çukurova University, Physics Department, Balcalı, 01330 Sarıçam, Adana, Turkey
[b] Kahramanmaras Istiklal University, Elbistan Vocational High School of Health Service, Elbistan, Kahramanmaras, Turkey
[c] Hasan Kalyoncu University, Faculty of Engineering, Department of Electrical and Electronics Engineering, Gaziantep, Turkey
[d] Institute of Physics, Polish Academy of Sciences, Al. Lotnikow 32/46, 02-668 Warsaw, Poland

ARTICLE INFO

Article history:
Received 9 February 2021
Received in revised form 14 April 2021
Accepted 20 April 2021
Available online 29 April 2021

Keywords:
BeO
Lanthanides
Ceramic phosphors
Radioluminescence
Thermoluminescence
Optically stimulated luminescence
Clinical dosimetry

ABSTRACT

This work aimed to investigate the luminescent characteristics of lanthanide and alkali metal ion-doped BeO ceramic pellets prepared using the co-precipitation synthesis technique for Optically Stimulated Luminescence (OSL) dosimetry applications. In this study, BeO nano phosphor was doped with lanthanides (Ln^{3+}) Eu^{3+}, Ce^{3+}, Nd^{3+}, Yb^{3+}, Er^{3+}, Gd^{3+}, Tb^{3+}, Tm^{3+}, Sm^{3+}, Pr^{3+}, and Dy^{3+} and co-doped with Na^{+}, and characterized using radioluminescence (RL), thermoluminescence (TL) and OSL techniques. Lanthanides introduced as dopants not only affected the luminescence centers but also changed the luminescence mechanisms. The RL spectra of lanthanide-doped BeO samples showed that they mostly possess dominant emissions in the narrow bands (between 200 and 450 nm) in the UV region. OSL emission bands were found to be located between ~250 and ~390 nm. The results have demonstrated that the incorporation of appropriate Ln^{3+} and alkali metal ion dopants and their optimum concentrations enhanced the luminescence intensity of undoped BeO. The studied BeO:$Na_{5\%}$,$Ce_{0.01\%}$,$Er_{0.01\%}$, BeO:$Na_{5\%}$,$Ce_{0.005\%}$,$Tb_{0.05\%}$, and BeO:$Na_{5\%}$,$Ce_{0.01\%}$,$Dy_{0.01\%}$ ceramics can be regarded as highly sensitive controllable luminescence dosimeters. The range of sensitivity of those samples is such that their most probable use in clinical therapy dosimetry rather than in health physics.

1. Introduction

The entire phenomena of luminescence of insulating and semiconducting materials include the excitation of charged carriers, charge carrier migration, and trapping at defect centers; the thermal or optical release of the trapped charge carriers; and finally the recombination of the charge carriers resulting in luminescence. Arising the electron-hole recombination causes excitation of luminescence centers in the crystal which is followed by decaying to the ground state and simultaneous emission of the photons. The phenomenon is called Thermoluminescence (TL) if the stimulation mode is thermal, and Optically Stimulated Luminescence (OSL) if it is optical. The aforementioned process has been the basis for the practical use of TL and OSL in ionizing radiation detection and measurement.

To estimate absorbed radiation dose, TL, and OSL materials as passive detectors are used in radiation dosimetry [1–7]. Luminescence of dosimetric materials is controlled using appropriate dopant ions generally transition metal and/or rare-earth metal ions as the luminescent centers. Such dosimeters should have features of high sensitivity to radiation, light-sensitive trapped charges, low-fading at room temperature, insensitivity to external influences such as humidity or mechanical stress, and possibly easy and fast readouts. Besides, features such as soft tissue equivalency for Z_{eff} value, minimum size, or cost may be important for the commercialization of the product. In the literature, although there are a lot of materials with well-determined OSL properties (Al_2O_3, BeO, MgO, etc.), there exist a limited number of commercialized OSL materials e.g., Al_2O_3:C from Landauer Inc. and Thermalox 995 BeO from Materion Inc. For this reason, the researchers have suggested fundamental mechanisms governing the luminescence properties in various host oxide lattices and developed new TL or OSL materials [8–18].

With a wide bandgap of approximately 10.6 eV, BeO as an insulator has been used commercially in industrial applications since

* Corresponding author.
E-mail address: valtunal@cu.edu.tr (V. Altunal).

https://doi.org/10.1016/j.jallcom.2021.160105
0925-8388/

the 1950s. It has many unique structural, chemical, and physical properties [19,20]. Specifically, BeO ceramic dosimeters are widely used in personal dosimetry applications because they have a low-effective atomic number (Z_{eff} = 7.13) that is quite close to biological tissue (Z_{eff} = 7.42). In the first dosimetric studies performed with BeO, the material was proposed as alternative thermoluminescence (TL) dosimeter to TLD-100 dosimeter. However, due to the toxicity of BeO powders and high light sensitivity of TL signals, important difficulties in using the material in TL applications have been revealed [2,5,21]. Although these light-sensitive TL signals in BeO seemed to be a disadvantage in practice, in later times they encouraged many researchers for the usage of the BeO ceramics in OSL applications [22]. After the detailed OSL study of BeO (Thermalox 995 chip) [23], the material has become popular among researchers for OSL dosimetry. As a result of ongoing researches, a commercialized BeO-based OSL dosimetry system has been produced for radiation dosimetry [24–27].

BeO Thermalox 995 OSL material from Materion Ceramics is a widely used commercial dosimeter in research and has been described in the literature [24,28]. BeO Thermalox 995 chips contain many transition metal impurities such as Si, Mg, Fe, Al, B, and Ca [29,30]. As these elements are not specifically doped to the material for dosimetric purposes, understanding and controlling the luminescence characteristics of the material are complicated. Therefore, it attracts researchers to produce new BeO-based materials with appropriate dopants to improve the luminescence properties of BeO ceramic material and achieve controllable luminescence. Due to the increasing demand for passive radiation detectors in radiation dosimetry, our research group has been studying synthesized and doped BeO ceramics as probable OSL dosimeters over the last decade [11–13,20,31,32].

Lanthanide (Ln) ions have been extensively studied in recent years for their potential use as lighting elements [33]. Complicated optical characteristics of Ln ions originate primarily from the unique features of their electronic [Xe]$4f^N$ configurations (N = 0–14), which have very localized states and can be represented in the theory of the crystal-field conventionally. In particular, Ln^{3+} based upconversion (UC) luminescence is one of the most important properties of rare-earth luminescence, which has attracted attention in materials science to understand defects in materials, in recent years [34]. Upconversion, which is a nonlinear anti-Stokes process, is briefly the conversion of low-energy near-infrared (NIR) photons into higher-energy photons (ultraviolet (UV), visible, and NIR) [35]. This conversion takes place by using actual ladder-like energy levels divided by the electric field effect generated by the crystalline environment, and the use of the long lifetime of Ln^{3+} ions located in a suitable dielectric crystal [33,36,37]. The enhancement of UC luminescence is of significance for the production of luminescent materials suitable for desired application areas. Specifically, luminescence of lanthanide (Ln^{3+}) ions doped BeO has been seldomly studied. Furthermore, there are few works of literature about lanthanide (Ln^{3+}) ions doped BeO, and the luminescent properties of these materials haven't been systematically investigated yet.

This work was particularly done to achieve the enhanced luminescence in BeO ceramic samples by the optimization of the Ln^{3+} dopant concentrations, and application of the passive admixtures (e.g., Na^+, Li^+, K^+ co-doping). We developed alternative BeO oxide phosphors with better efficiency and extended their applications to be used in luminescence dosimetry. In this work, lanthanides (rare-earth elements) Eu^{3+}, Ce^{3+}, Nd^{3+}, Yb^{3+}, Er^{3+}, Gd^{3+}, Tb^{3+}, Tm^{3+}, Sm^{3+}, Sr^{3+}, Pr^{3+}, and Dy^{3+} doped BeO ceramic samples were successfully produced using the co-precipitation method and interpretation of their luminescence mechanisms was proposed. Luminescence characteristics of the Ln^{3+}-doped BeO samples were studied using OSL spectra, radioluminescence (RL), TL, and OSL techniques. Luminescent behaviors were investigated in terms of possible relations to the trivalent lanthanide dopants and alkali metal ion co-dopants added into the BeO host material.

2. Material and method

2.1. Material synthesis

BeO ceramics were synthesized and doped using the co-precipitation method. Beryllium sulfate tetrahydrate (99.90%, $BeSO_4$•$4H_2O$), polyethyleneimine solution ($(NHCH_2CH_2)_n$, 50% (w/v) in H_2O), and ammonium hydroxide (28.0–30.0% NH_3 basis, NH_4OH) precursor reactants were used for initial salt, polymerization, and initiator of the precipitate, respectively. All raw dopant materials (Na^+, Li^+, K^+, and Ln^{3+} (Eu^{3+}, Ce^{3+}, Nd^{3+}, Yb^{3+}, Er^{3+}, Gd^{3+}, Tb^{3+}, Tm^{3+}, Sm^{3+}, Sr^{3+}, Pr^{3+}, and Dy^{3+})) used were only nitrate based. The co-precipitation method was presented in detail previously in our studies [12,20,31,38], and modified to better control the Ln^{3+}-doped BeO synthesis process in this study. The actual Ln^{3+} contents in the sintered pellets were not verified. The resultant precipitate samples were calcined at 900 °C for 4 h in the air atmosphere for removing the organic formations which come up with the synthesis process and obtaining the BeO nanocrystal structure of the material. Finally, lanthanide-doped BeO powders were prepared in pellet forms to obtain more settled OSL signals. BeO ceramic pellets having dimensions of ~3.1 mm radius and ~0.8 mm thickness were obtained using 25 mg powder samples. To avoid the toxicity of BeO powders, and provide strength and integrity, the prepared pellets were sintered at 1600 °C for 4 h. After sintering, the weight losses were observed and the average weights appeared as ~23.1 ± 0.2 mg. Inhalation of beryllium powders in the air may cause a serious lung condition, depending on the dose. It should be noted that, unlike BeO powders, the use of solid form BeO ceramics (chips, rods, discs, etc.) does not pose a special health risk. In our work with BeO, we paid attention to safety and environmental protection studies to avoid toxicity and followed safe usage practices. Personal protective equipment such as gloves, dust/gas masks, and/or goggles was used during BeO synthesis.

2.2. Characterization techniques

Powder x-ray diffractograms (XRD) were obtained using a PANalytical EMPYREAN XRD diffractometer with Cu-Kα (the generator voltage of 60 kV, the current of 40 mA) by scanning from 10° to 90° (2θ) with 0.02° (2θ) steps. The XRD patterns were compared with the reference data by the International Centre for Diffraction Data (ICDD). The Raman spectra of undoped and Ln^{3+} doped BeO ceramics were done using a Raman spectrophotometer (Renishaw in Via Qontor) with 532 nm laser as excitation wavelength.

A DA-20 model RisØ TL/OSL reader system was used for the TL and OSL measurements. The samples were irradiated using a ^{90}Sr-^{90}Y beta particle source. TL and OSL emissions in the UV region were detected using a Hoya U-340 filter in front of the bialkali photomultiplier tube (PMT) unit. In OSL readouts, samples were firstly irradiated with a 0.5 Gy beta dose and preheated to 100 °C for 10 s for eliminating the signals that come from the shallow traps. 470 nm Blue LEDs were used for the light stimulation for 200 s in continuous wave OSL mode (CW-OSL mode). TL readouts were conducted by heating the previously irradiated samples with 0.5 Gy dose to 650 °C without any preheating. In all the TL measurements, the heating rate was 3 °C/s. Before TL/OSL comparison measurements of Ln^{3+}-doped BeO ceramics, each sample was individually calibrated according to a reference dose of 0.5 Gy to better identify variations in responses in the same batch. All the experimental data reported in this study is presented after a correction made using obtained calibration factors. To increase the reliability of the

luminescent experiments, both the fresh pellets and used pellets were measured after annealing at 650 °C for 10 min

RL analyzes of the Ln^{3+}-doped BeO ceramics were obtained using a handmade radioluminescence system equipped with a highly sensitive Ocean Optics fiber spectrometer, a CCD detector. Ln^{3+} doped BeO ceramic samples were exposed to X-rays of ~20 kV.

OSL emission spectra were measured using a Horiba Jobin-Yvon Fluorolog-3 spectrofluorometer with a 450 W continuous xenon lamp for excitation and optical detection with a Hamamatsu R928P photomultiplier operating in the photon counting mode. The excitation monochromator was set to 475 nm and the emission spectra were recorded by scanning from 240 to 420 nm in 3 nm increments using 0.1 s integration time. The slits of excitation and emission were selected as 5 nm and 9.5 nm, respectively. A 450 nm long-pass filter for excitation and an UFS-1 short-pass filter were used. The excitation time was 60 s. All the OSL emission spectra presented here were previously corrected by the spectral response of the system. To reduce the effect of change over time, all spectra were recorded as quickly as possible, and each was averaged after 3 consecutive scans.

3. Results and discussion

3.1. Crystal structure

The crystallographic phase formation of BeO was confirmed by comparing it with the ICDD PDF-card no 98–001–5620 revealing the hexagonal crystal structure with the $P6_3mc$ space group. Fig. 1. shows the well-indexed three highly sensitive peaks with (100), (002), and (101) orientations from undoped and Ln^{3+}-doped BeO ceramics. The XRD patterns showed that BeO ceramics doped with different Ln^{3+} ions synthesized under the same synthesis processes (i.e., calcination and sintering conditions) had the same phase. The XRD patterns do not contain any peaks related to Ln^{3+} ions, this may be attributed to the incorporation of Ln^{3+} ions into Be^{2+} lattice sites rather than interstitial ones [39].

Apart from the general appearance of XRD patterns, lattice parameters were evaluated from the XRD data. As expected from the difference in ionic radii between Ln^{3+} and Be^{2+} host sites (see Appendix A. Table A1.), a systematic change in lattice parameters was observed in Table 1. Both lattice parameters (a and c) and cell volume (V) were decreased with Ln^{3+}doping due to an increase in the existing defect concentration in the lattice. This may be attributed to the larger ionic radius of Ln^{3+} compared to that of Be^{2+}, hence leading to a lattice contraction [39,40]. Furthermore, The Be-O bond length values obtained from the XRD data of the BeO:Ln^{3+} samples are slightly lower than that of the undoped BeO sample (see Table 1.), indicating that the structural defects and especially the oxygen vacancies have been reduced. The oxygen positional parameter (u) and c/a values providing information about the oxygen vacancies in the structure were also evaluated. All the BeO:Ln^{3+} samples showed a significantly higher c/a ratio than undoped BeO, which may indicate reduced oxygen vacancies V_O and extended defects (dislocations and grain-boundaries) [39].

On the other hand, the structural parameters, diffraction peak position (2θ), FWHM (β), the crystallite size (D), micro-strain (ε), and dislocation density (δ) of undoped and Ln^{3+}-doped BeO samples were evaluated from the XRD data and summarized in Table 2. As can be seen from Table 2, the diffraction peak positions (2θ) slightly shifted to the right with Ln^{3+}doping. It can be said that three highly sensitive peaks regarding (100), (002), and (101) orientations shift to the right due to a decrease in lattice parameters a and c when compared to the undoped sample, leading to a resultant increase in the concentration of defects in the structure [31,41]. In our investigations, as the target material was exposed to severe deformation with Ln^{3+} doping, the resulting deformation and inhomogeneous strain in the crystal lattice led to increase in

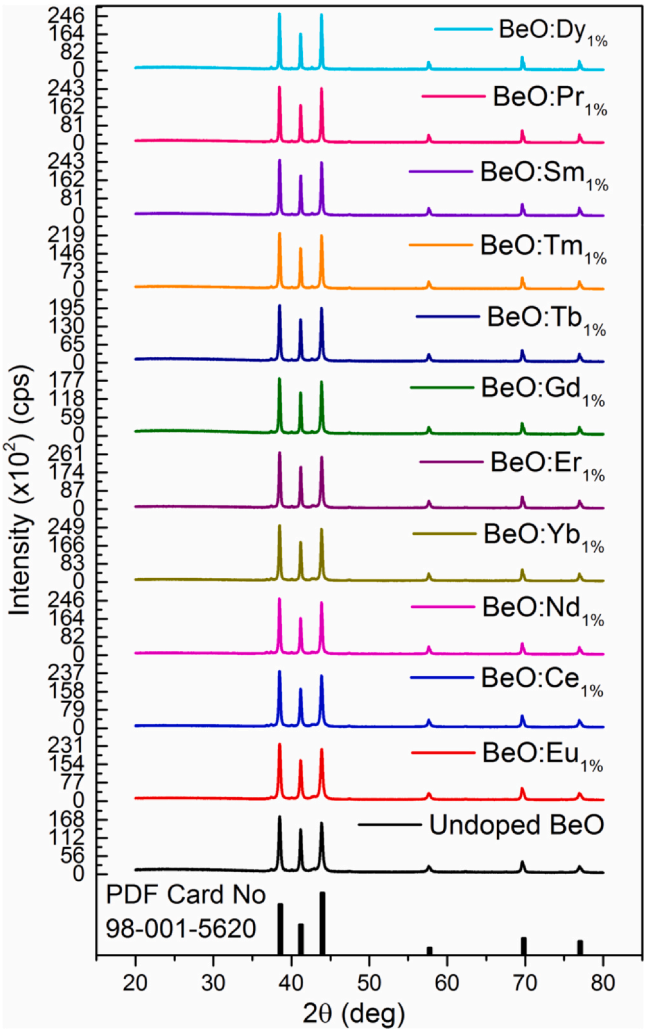

Fig. 1. XRD patterns of undoped and 1 mol% of Ln^{3+} doped BeO phosphors.

Table 1
Lattice parameters a and c, unit cell volume (V), lattice distortion c/a, positional parameter u and Be–O bond length L of undoped and Ln^{3+}-doped BeO samples synthesized by the co-precipitation method.

	Lattice Parameters			c/a	u	Be–O bond Length L (Å)
	a (Å)	c (Å)	V (Å³)			
BeO	2.459	4.388	22.97	1.7844	0.35468	1.55620
BeO:Eu	2.397	4.390	21.85	1.8313	0.34939	1.53385
BeO:Ce	2.397	4.385	21.82	1.8293	0.34962	1.53310
BeO:Nd	2.397	4.386	21.83	1.8298	0.34956	1.53329
BeO:Yb	2.397	4.386	21.83	1.8298	0.34956	1.53329
BeO:Er	2.397	4.386	21.83	1.8298	0.34956	1.53329
BeO:Gd	2.428	4.388	22.39	1.8074	0.35204	1.54461
BeO:Tb	2.428	4.388	22.39	1.8074	0.35204	1.54461
BeO:Tm	2.397	4.386	21.83	1.8298	0.34956	1.53329
BeO:Sm	2.428	4.386	22.39	1.8069	0.35210	1.54443
BeO:Pr	2.368	4.385	21.29	1.8521	0.34717	1.52239
BeO:Dy	2.459	4.388	22.97	1.7844	0.35468	1.55620

full-width at the half maximum (FWHM = β) of the diffraction peak (see Table 2). It has been observed that diffraction broadening causes generally an increase in lattice micro-strain (ε) and a decrease in crystallite size (D) of strain-hardened materials. This is an indication of an increase in the overall defect concentration in the structure. Whereas, by adding Yb^{3+}, Pr^{3+}, and Dy^{3+} dopants, while the crystal grew in preferred orientations, it caused a decrease in micro-strain, which means a low lattice imperfection in the structure (see

Table 2
Structural parameters, diffraction peak position (2θ), FWHM (β), crystallite size (D), micro-strain (ε) and dislocation density (δ) of undoped and Ln^{3+}-doped BeO samples synthesized by the co-precipitation method.

	2θ (°)			β (°)			D (nm)			ε x 10^{-2}			δ x 10^{-3} (nm^{-2})		
	(100)	(002)	(101)	(100)	(002)	(101)	(100)	(002)	(101)	(100)	(002)	(101)	(100)	(002)	(101)
BeO	38.44	41.15	43.83	0.1839	0.1714	0.1922	47.8	51.73	46.55	4.286	4.011	4.457	0.438	0.374	0.461
BeO:Eu	38.46	41.13	43.83	0.3745	0.5379	0.2525	23.48	16.48	35.44	8.693	12.589	5.856	1.814	3.682	0.796
BeO:Ce	38.46	41.17	43.85	0.1955	0.1721	0.2101	44.97	51.52	42.59	4.538	4.028	4.872	0.494	0.377	0.551
BeO:Nd	38.46	41.16	43.84	0.2649	0.2159	0.2953	33.19	41.07	30.3	6.149	5.053	6.849	0.908	0.593	1.089
BeO:Yb	38.46	41.16	43.85	0.209	0.1721	0.2215	51.08	51.52	40.4	4.851	4.028	5.137	0.383	0.377	0.613
BeO:Er	38.46	41.16	43.84	0.2682	0.2543	0.3002	32.78	34.87	29.81	6.226	5.951	6.961	0.931	0.822	1.125
BeO:Gd	38.45	41.15	43.84	0.2035	0.1782	0.2089	43.2	49.76	42.83	4.733	4.171	4.845	0.536	0.404	0.545
BeO:Tb	38.45	41.15	43.84	0.1847	0.1457	0.1928	47.6	60.85	46.41	4.296	3.410	4.471	0.441	0.270	0.464
BeO:Tm	38.46	41.16	43.85	0.1841	0.1847	0.1868	47.75	48.01	47.9	4.273	4.323	4.332	0.439	0.434	0.436
BeO:Sm	38.45	41.16	43.83	0.2776	0.2542	0.2177	31.67	34.88	41.1	6.457	5.949	5.049	0.997	0.822	0.592
BeO:Pr	38.47	41.18	43.86	0.1507	0.1459	0.1493	58.34	60.82	59.94	3.491	3.414	3.463	0.294	0.270	0.278
BeO:Dy	38.44	41.15	43.83	0.1334	0.1234	0.1352	65.9	65.58	67.07	3.109	2.888	3.136	0.230	0.233	0.222

Table 2.). The calculated dislocation densities increased with Ln^{3+} doping, and consequently, dislocation movements occurred at higher dislocation densities for the doping process. The effect of doping of Ln^{3+} ions having larger ionic radii on the stress and dislocation densities in the synthesized BeO structures is clearly seen in Table 2. Larger dislocation density may be associated with greater hardness or a decrease in particle size [42,43]. As a result of these phase analyzes, it was found that the crystallinity, defect structures, and physical properties of the BeO ceramics depend strongly on the Ln^{3+} dopants. A detailed description and model equations related to lattice and structural parameters were presented in Appendix A.

Fig. 2 shows the Raman spectra of the undoped and Ln^{3+} doped BeO ceramics excited by a laser with a wavelength of 532 nm. Two major peaks of A_1 (TO) (680.23 cm^{-1}) and E_1 (TO) (722.21 cm^{-1}) optical phonons were detected on all samples. Additionally, a low sensitive peak of A_1 (TO) optical phonon was observed between 1085.85 cm^{-1} and 1096.56 cm^{-1}. Theoretical calculations for the E_1 and A_1 phonon modes, which are originated from the opposite motion of the Be and O bond in the basal plane, were reported as 697–725 cm^{-1} and 1080–1113 cm^{-1} [44,45]. The E_1 mode oscillates perpendicular to the c-axis, while the A_1 mode oscillates parallel to the c-axis. It can be said that the BeO phase did not change with Ln^{3+} doping, and thus Ln^{3+} ions successfully entered the BeO lattice because no additional peaks associated with the Ln^{3+} ions were observed in Raman spectra (see Fig. 2). Therefore, Ln^{3+} ions can be suggested that they substitute for Be^{2+} lattice sites rather than locate in interstitial positions.

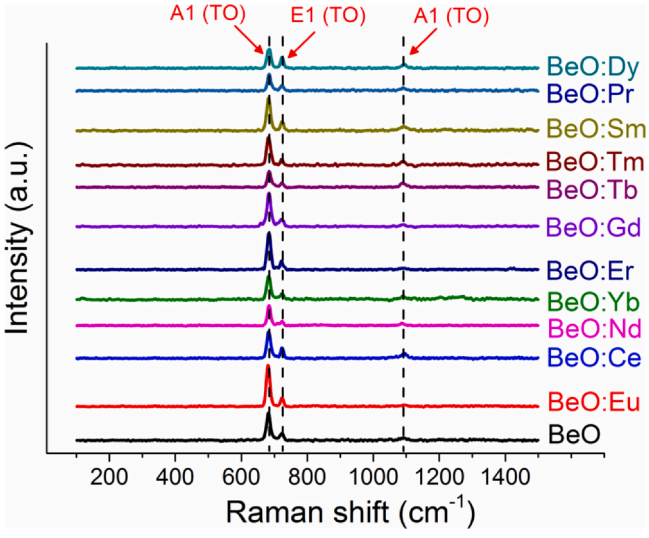

Fig. 2. Raman spectra of undoped and Ln^{3+} doped BeO ceramics measured using 532 nm laser.

3.2. RL emissions of undoped and single-doped BeO

It is well known that the optical characteristics and the emission intensity of Ln^{3+} ions are very sensitive to the surrounding crystal structure and crystal field environment. Investigation of RL properties of Ln^{3+} doped nanocrystals is thereby important to provide knowledge about the locations and overview of luminescence bands. In this study, RL emissions of the undoped and singly doped BeO ceramics, with lanthanides at 1 mol% dopant concentration, namely, $BeO:Eu_{1\%}$, $BeO:Ce_{1\%}$, $BeO:Nd_{1\%}$, $BeO:Yb_{1\%}$, $BeO:Er_{1\%}$, $BeO:Gd_{1\%}$, $BeO:Tb_{1\%}$, $BeO:Tm_{1\%}$, $BeO:Sm_{1\%}$, $BeO:Pr_{1\%}$, and $BeO:Dy_{1\%}$ were obtained using a 1 nm resolution at room temperature and presented in Fig. 3.

All the lanthanide-doped BeO ceramic samples were found to exhibit a characteristic wide UV emission band of BeO with a maximum at 250 nm, located between 200 and 450 nm (see Fig. 3). The source of the large and sensitive emission at approximately 4.9 eV is the radiative annihilation of self-trapped excitons caused by X-ray excitation [31,32,46,47]. The luminescence in BeO is known to be characterized by the two emission bands at ~3–4 eV (300–400 nm) and 4.9 eV [47]. Because the 4.9 eV emission band is not close to the spectral range of the conventional PMT and transmission range of the Hoya U-340 filter, herein, only 3–4 eV emission bands were observed in OSL readouts. In the literature, the sources of RL and OSL emissions in a Thermalox BeO chip were reported to be different, and the resulting luminescence mechanisms in BeO were suggested to be different [48]. However, in our studies, the RL and OSL emissions were found to be similar for synthesized Ln^{3+} doped BeO ceramics (will be discussed later).

Eu^{3+}-doped BeO ceramics showed typical RL emission bands of Eu^{3+} ions located between 570 and 750 nm (see Fig. 3b), which could be ascribed to $^5D_0 \rightarrow {}^7F_j$ ($j = 0 - 4$) red emission transition of Eu^{3+}. The characteristic emission of Eu^{2+} at 384 nm, which originated from the $5d \rightarrow 4f$ transition, was not observed because it remains under the main emission peak of BeO. In the case of Ce^{3+}-doped BeO ceramics, although RL emission bands located between ~300 nm and 450 nm ($5d \rightarrow 4f$ transition) did not appear as isolated peaks and probably located under the dominant broadband emission of BeO. As is shown in Fig. 3c, doping with Ce^{3+} ions caused an increase in the intensity of characteristic peaks in the RL diffractogram. 400 nm RL emission peak was observed from the Nd^{3+}-doped BeO ceramics (see Fig. 3d), associated with the $4f \rightarrow 4f$ transitions of Nd^{3+}. In Fig. 2e, Yb^{3+}-doped BeO samples showed a characteristic emission centered at 525 nm, originated from the allowed electric dipole $5d \rightarrow 4f$ transition of Yb^{2+}. The observed emission peak at ~570 nm in Fig. 2f represents the $^4S_{3/2} \rightarrow {}^4I_{15/2}$ characteristic transition of Er^{+3}. In Fig. 3g,

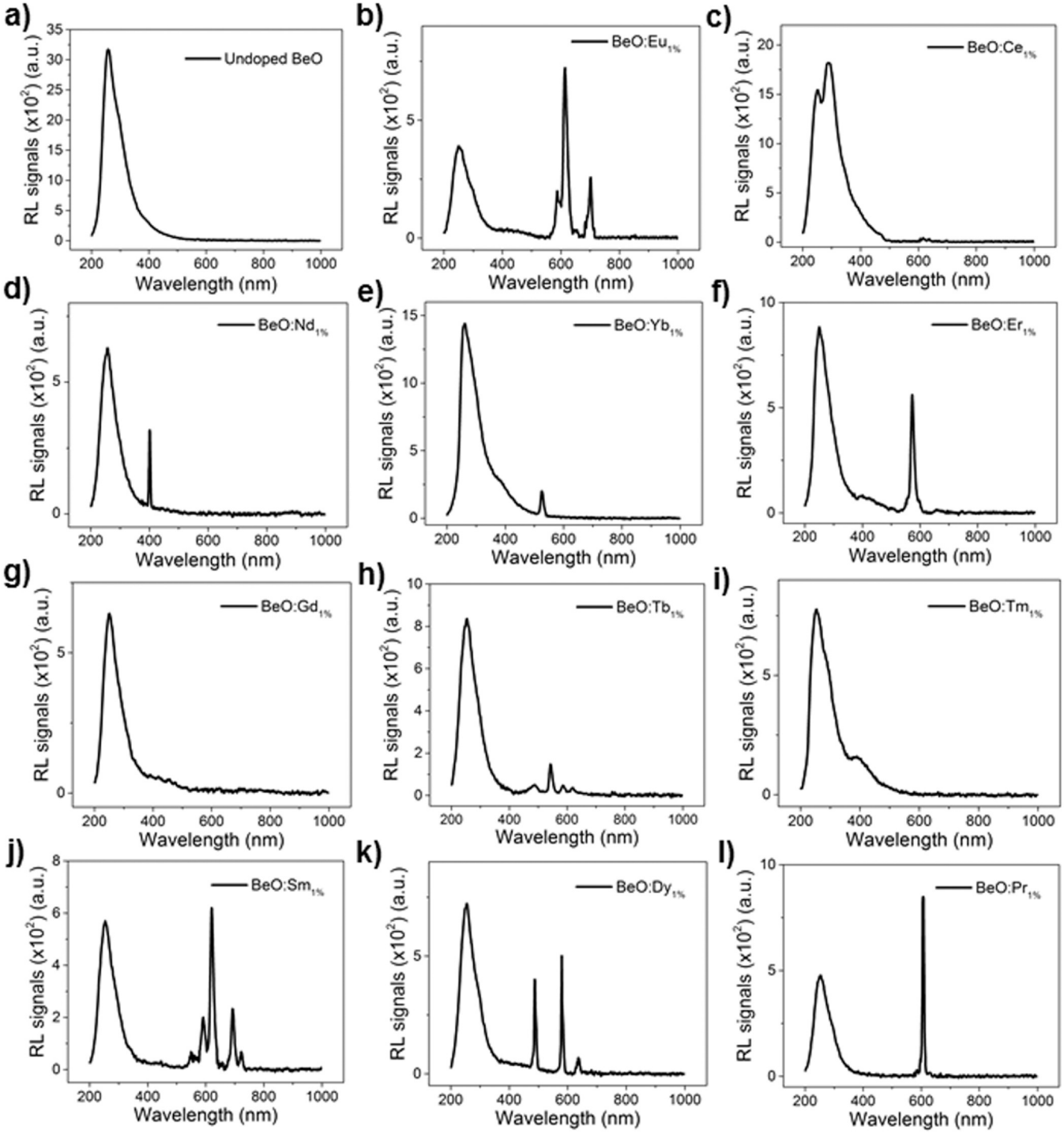

Fig. 3. The RL emission spectra of undoped BeO and BeO:$Ln_{1\%}$ ceramic samples a) undoped BeO, b) BeO:$Eu_{1\%}$, c) BeO:$Ce_{1\%}$, d) BeO:$Nd_{1\%}$, e) BeO:$Yb_{1\%}$, f) BeO:$Er_{1\%}$, g) BeO:$Gd_{1\%}$, h) BeO:$Tb_{1\%}$, i) BeO:$Tm_{1\%}$, j) BeO:$Sm_{1\%}$, k) BeO:$Pr_{1\%}$, and l) BeO:$Dy_{1\%}$. Samples were sintered at 1600 °C for 4 h after calcination at 900 °C for 4 h.

the characteristic 315 nm RL emission is likely to be associated with the $^6P_{7/2} \rightarrow {}^8S_{7/2}$ transition of Gd^{3+}. This RL emission was observed in the RL spectra of BeO: Gd^{3+} samples as overlapping with the dominant emission of BeO. For the Tb^{3+}-doped BeO samples in Fig. 3h, at least six overlapped peaks in the visible region were observed in RL spectra. It can be said that these visible range emission peaks are due to the $^5D_4 \rightarrow {}^7F_j$ ($j = 6 - 0$) characteristic transitions of Tb^{3+} with the emission bands located at 490, 540, 580, 620, 650, 660 and 675 nm [49]. Only Tm^{3+}-doped BeO ceramics showed a distinct peak with a maximum of about 400 nm occurred as a neck at the right side of the 250 nm broad emission peak of pure BeO (see Fig. 3i). This 400 nm RL emission is due to the $^1D_2 \rightarrow {}^3F_4$ transition of Tm^{3+}. Sm^{3+}-doped BeO samples showed five characteristic RL emission bands located at 560, 595, 640, 700, 775 nm (see Fig. 3j), which are denoted by the $^4G_{5/2} \rightarrow {}^6H_j$ ($j = 5/2 - 13/2$) transitions of Sm^{3+}. The observed characteristic emission from the Pr^{3+}-doped BeO ceramics was at ~600 nm in Fig. 3k, and corresponds to the $^1D_2 \rightarrow {}^3H_4$ transition of Pr^{3+}. Three RL emission bands located at 475, 570, and 660 nm in Dy-doped BeO samples were observed that they originate from the $^4F_{9/2} \rightarrow {}^6H_j$ ($j = 15/2 - 11/2$) transitions of Dy^{3+}

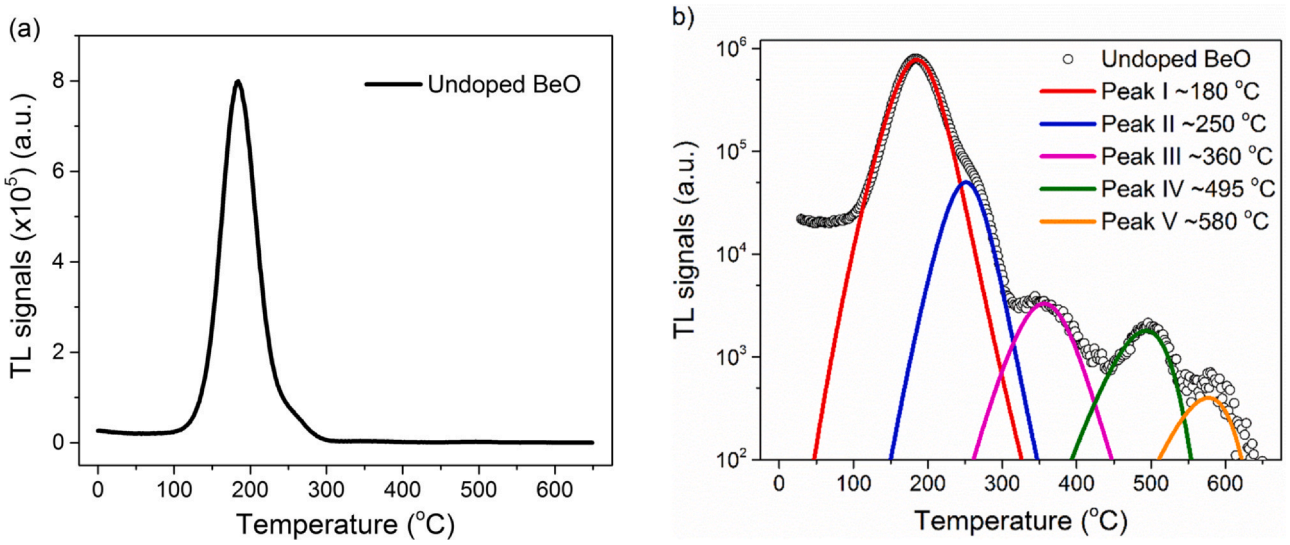

Fig. 4. TL glow curve of undoped BeO: (a) TL signals in linear scale, (b) Deconvoluted TL signals in semi-log scale.

(see Fig. 3l). As a result, peaks corresponding to the characteristic transitions of trivalent lanthanide ions showed that each Ln^{3+} ion plays a role as a luminescence center in the BeO structure.

Another important revealing of RL emissions obtained with lanthanide doping in the BeO structure is a diminution of the luminescence at wavelengths between 200 and 400 nm when compared with the RL emission intensity of undoped BeO (see Fig. 3). This might be caused by the quenching effect of defect-related Ln^{3+} emissions and the unmatched energy levels relative to the valence (VB) and conduction bands (CB) of BeO. These effects have been mentioned in the literature for various oxide nanocrystal hosts [50].

3.3. TL glow curves of undoped and single-doped BeO

The TL glow curve of undoped BeO revealed five peaks at ~180, ~250, ~360, ~495, and ~580 °C with a heating rate of 3 °C/s (see Fig. 4). In Fig. 4a, a highly sensitive TL peak at ~180 °C possessing its maximum height being ~10^3 times greater than the peak was observed on the high-temperature side of the glow curve. For a better illustration of the low sensitive traps, TL glow curves were deconvoluted and component peaks were given in Fig. 4b. On the other hand, studies on the TL glow curve of BeO Thermalox 995 chip showed three main TL peaks at 75, 200, and 340 °C (depending on the heating rates during TL readouts) [23], although some deep traps were also found after 340 °C [51]. In this work, the observed five peaks are suggested to be consistent with the TL glow curve shapes obtained in the undoped and doped BeO ceramic materials specified in our previous studies [12,13,31].

To investigate the effect of lanthanide doping on TL glow curves of BeO ceramics, TL readouts were carried out by heating the samples exposed to 0.5 Gy beta dose up to 650 °C with a heating rate of 3 °C/s without any preheating procedure. Fig. 5 shows the TL glow curves of BeO ceramics singly doped with lanthanides at 1 mol% dopant concentration, namely, BeO:$Eu_{1\%}$, BeO:$Ce_{1\%}$, BeO:$Nd_{1\%}$, BeO:$Yb_{1\%}$, BeO:$Er_{1\%}$, BeO:$Gd_{1\%}$, BeO:$Tb_{1\%}$, BeO:$Tm_{1\%}$, BeO:$Sm_{1\%}$, BeO:$Pr_{1\%}$, and BeO:$Dy_{1\%}$. As can be seen in Fig. 5, all measured TL curves possess the four of five characteristic peaks of undoped BeO at ~180, ~360, ~495, and ~580 °C in varying intensities. A low sensitivity shallow peak at 60 °C was recorded in the Nd^{3+}, Yb^{3+}, and Tm^{3+}doped BeO samples. While all Ln^{3+} dopants activated the traps located between 300 and 400 °C, Yb^{3+}, Tb^{3+}, Tm^{3+}, and Pr^{3+} doped BeO affected the traps in the neighborhood of 180 °C TL peak. The high-temperature portion of the glow curve exhausted at 495 and 580 °C, and improved only via Ce^{3+} and Gd^{3+} dopant ions. In addition, a shoulder peak appearing around 250 °C in undoped BeO sample was not observed with the Ln^{3+} ions doping (see Fig. 5). In certain cases, lanthanide doping has created TL peaks at higher temperatures (see Fig. 5). These newly observed TL peak formations may be related to the distortion in the BeO lattice produced by the Ln^{3+} ions that substitute for the Be^{2+} ions and originated from other intrinsic defects. Results indicate that Ln^{3+} ions act as luminescence centers during the TL process, as observed by their RL emissions.

The effect of the lanthanide concentrations on the glow curves of these ceramic samples was also investigated using 0.01%, and 0.1% molar ratios to optimize the luminescence efficiency. As the concentration of Ln^{3+} ions was decreased, the main peak intensity, together with the low and higher temperature peaks were increased. In this study, Ce^{3+} with 0.01% mol concentration was chosen as a promising dopant for BeO host matrix. Herein, it was shown that not only its high-temperature peaks but also the peaks below 250 °C were activated by Ce^{3+} ions.

3.4. OSL decay curves of undoped and single-doped BeO

The effect of Ln^{3+} doping on the OSL characteristics of undoped BeO ceramics was examined. All the OSL decay curves were recorded after 0.5 Gy irradiation at room temperature at a rate of 10 data points per second using 200 s blue light stimulation. Fig. 6 shows the OSL decay curves of undoped and single Ln^{3+}-doped BeO ceramics with their decaying components. As can be seen from Fig. 6, lanthanide dopings significantly affect the OSL behaviors (shapes and intensities of the OSL curves) when compared to that of the undoped BeO ceramics. The general appearance of OSL signals showed that all undoped and single Ln^{3+}-doped BeO ceramics have two time-decaying components (fast and slow).

The analyzes of the OSL decay curves were examined via a method by fitting to the combination of the time-decaying functions which is one of the most common methods using the general order kinetic approach [11,12,20,52]. The used fitting equation for the analyzes can be written as:

$$y = background\ (bkg) + 1^{st}\,(fast)component + 2^{nd}(slow)component$$

$$I(t) = bkg + I_1\left[1 + (b_1 - 1)\frac{t}{\tau_1}\right]^{-\frac{b_1}{b_1-1}} + I_2\left[1 + (b_2 - 1)\frac{t}{\tau_2}\right]^{-\frac{b_2}{b_2-1}} + \ldots \quad (1)$$

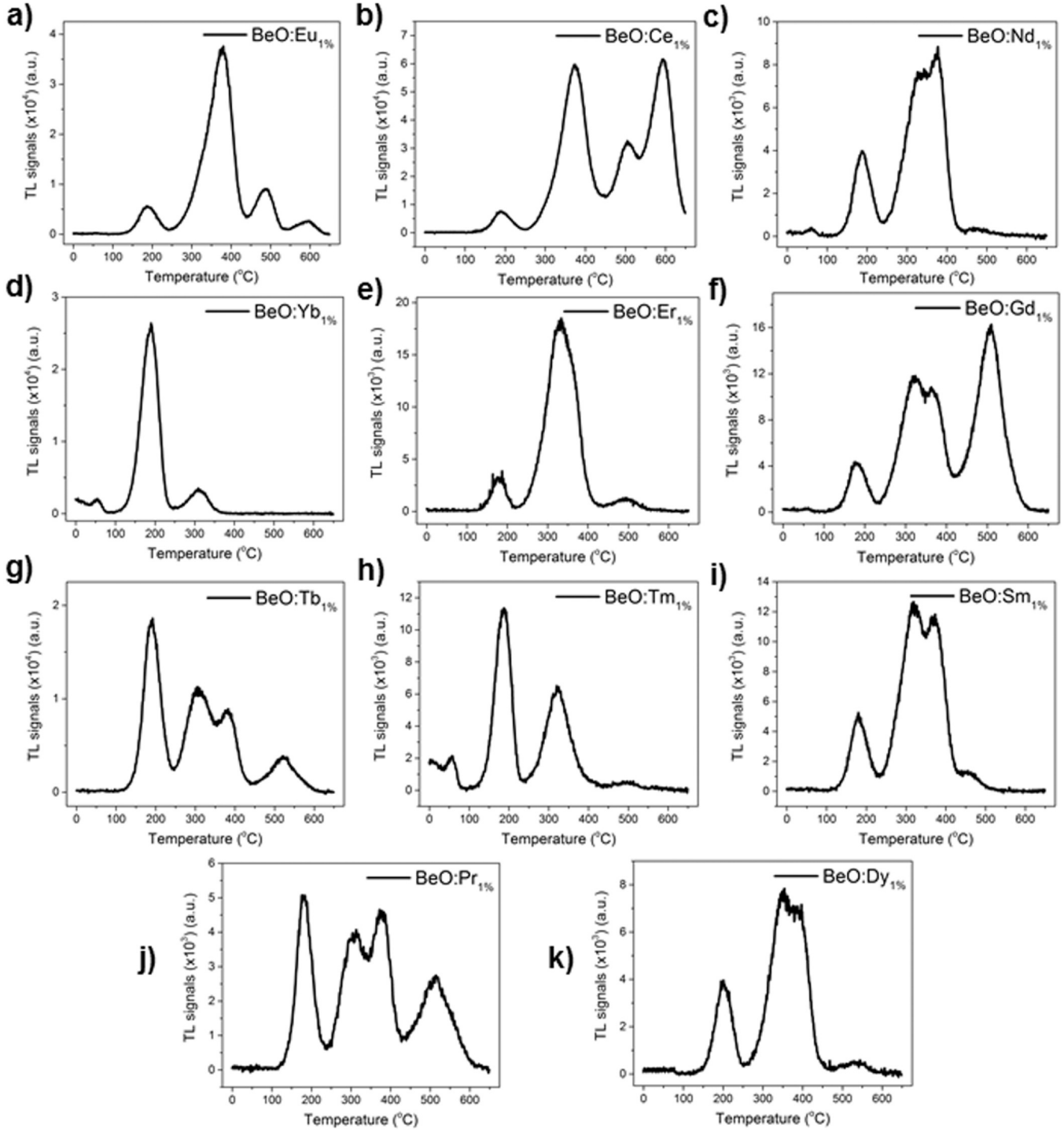

Fig. 5. The TL glow curves from BeO:$Ln_{1\%}$ ceramic samples, a) BeO:$Eu_{1\%}$, b) BeO:$Ce_{1\%}$, c) BeO:$Nd_{1\%}$, d) BeO:$Yb_{1\%}$, e) BeO:$Er_{1\%}$, f) BeO:$Gd_{1\%}$, g) BeO:$Tb_{1\%}$, h) BeO:$Tm_{1\%}$, i) BeO:$Sm_{1\%}$, j) BeO:$Pr_{1\%}$, and k) BeO:$Dy_{1\%}$.

where 1^{st} and 2^{nd} are the general-order ($1 < b < 2$) time decaying components representing the fast and the slow decaying parts of the OSL signals, respectively. t is the stimulation time; $I(t)$ is the intensity of the OSL signals as a function of time; bkg is the background signal of the OSL reader. $I_{1,2}$, $\tau_{1,2}$ and $b_{1,2}$ are the amplitudes, lifetimes, and kinetic orders of the separate components, respectively. $I_{1,2}$, $\tau_{1,2}$ and $b_{1,2}$ values were calculated using Eq. (1) and given with the FOM values (goodness of the fitting) in Table 3.

First order-kinetic assumes that the rate of retrapping of charge that has been released from a trap is negligible compared to the rate of recombination [53]. In second-order kinetics, re-trapping is dominant [54]. The situation in which both situations are mixed is defined as general-order kinetics [55]. In this work, we examined the b values, which represent the transition probabilities between the traps, of the 1st (fast) and 2nd (slow) components of the OSL decay curves. As is seen from Table 3, the b values of the 1st components resembled the general-order kinetics with the values between 1.19 and 1.68 except for the BeO:$Tb_{0.01\%}$ which exhibited second-order kinetic characteristics with b = 2.05. With the b values of 2.05, 2nd (slow) decaying components exhibited the second-order kinetic

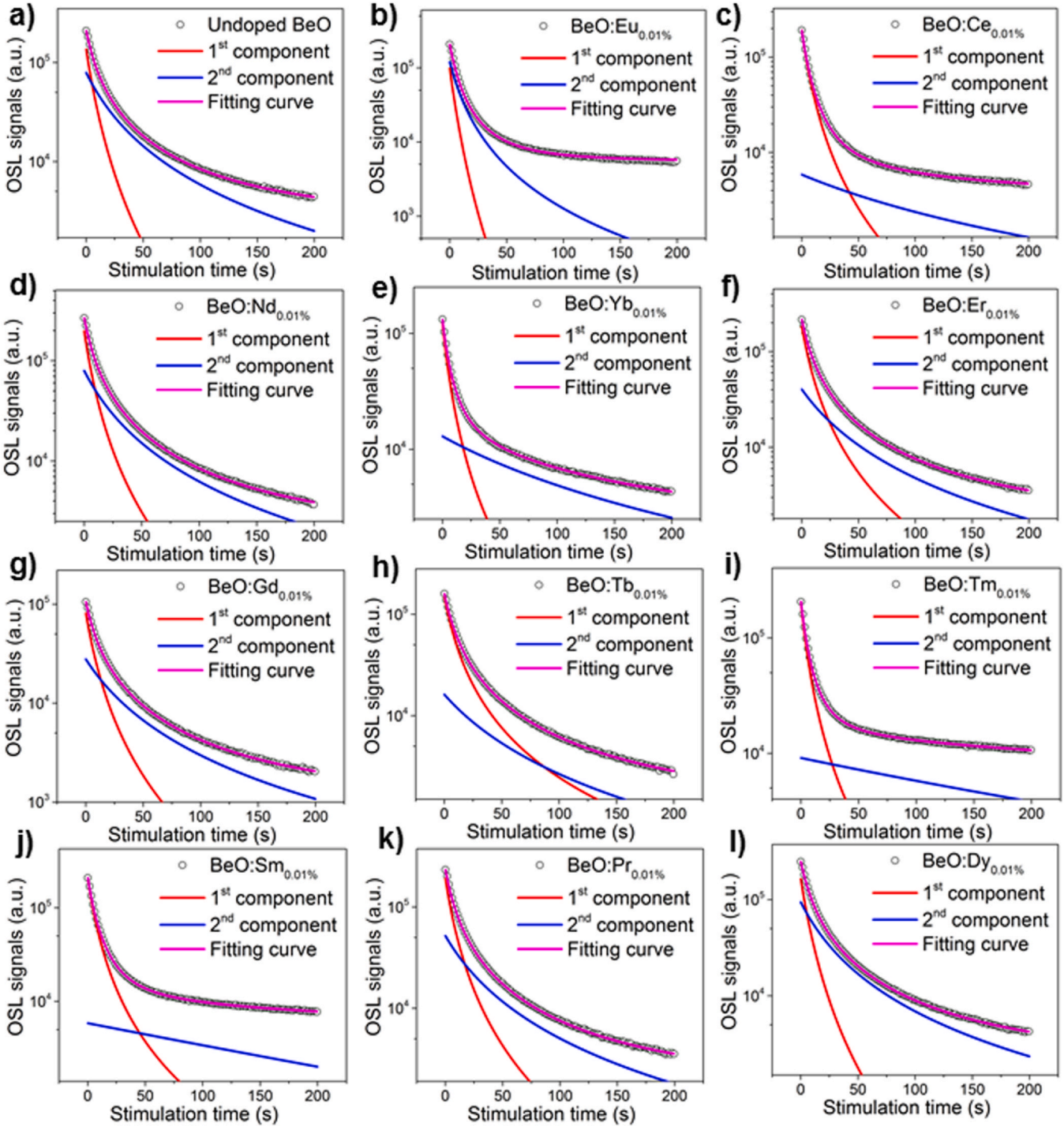

Fig. 6. The OSL decay curves and resultant components from the curve fitting of undoped BeO and BeO:$Ln_{1\%}$ ceramic samples a) undoped BeO, b) BeO:$Eu_{0.01\%}$, c) BeO:$Ce_{0.01\%}$, d) BeO:$Nd_{0.01\%}$, e) BeO:$Yb_{0.01\%}$, f) BeO:$Er_{0.01\%}$, g) BeO:$Gd_{0.01\%}$, h) BeO:$Tb_{0.01\%}$, i) BeO:$Tm_{0.01\%}$, j) BeO:$Sm_{0.01\%}$, k) BeO:$Pr_{0.01\%}$, and l) BeO:$Dy_{0.01\%}$.

characteristics (b = 2) except for BeO:$Eu_{0.01\%}$ and BeO:$Tm_{0.01\%}$ which demonstrated general-order characteristics (1 < b < 2). Only the 2nd components of OSL signals from the BeO:$Sm_{0.01\%}$ ceramics showed first-order kinetic behavior (b = 1.05).

When we worked over the lifetimes of the decay components, no serious differences were found in the τ_1 lifetime values of the 1st (fast)-decaying components of OSL signals. Whereas τ_2 lifetimes of the 2nd (slow) decaying components gave the changing values.

In our previous works, comparable OSL decay curves, and fitting parameters were found for the undoped and doped BeO ceramics [11,13,31]. In this work, the OSL decay curves of the studied materials were represented as the resultant of the two decaying curves. The number of time-decaying functions was reported as three for Thermalox BeO chips [23]. The results proved the existence of different types of defect centers and a more complex luminescence mechanism in the studied BeO materials. Therefore, these various types of defects in the BeO lattice structure cause a complex charge-carrier interaction between centers and localized bands. The TL and OSL mechanisms of the crystal can only be determined by the physical properties of the defect centers involved in (Ln^{3+} ions) and the kinetics associated with transition charge carriers. It should be remembered that this curve fitting is only an oversimplified

Table 3
$\tau_{1,2}$ decay times, $b_{1,2}$ kinetic orders and FOM values of the OSL decay fittings using two time-decaying functions for undoped and single lanthanide-doped BeO ceramics.

No.	1st (fast) component			2nd (slow) component				
	I_1 (count)	τ_1 (s)	b_1(a. u.)	I_2 (count)	τ_2 (s)	b_2(a. u.)	bkg (count)	FOM (%)
Undoped BeO	1.38E+05	7.73	1.36	7.94E+04	37.42	2.05	2.38E+03	0.55
BeO:Eu$_{0.01\%}$	1.01E+05	4.48	1.19	1.21E+05	12.46	1.74	5.45E+03	1.21
BeO:Ce$_{0.01\%}$	1.96E+05	7.62	1.54	5.87E+03	178.54	2.05	3.33E+03	0.79
BeO:Nd$_{0.01\%}$	2.01E+05	8.30	1.50	7.99E+04	38.99	2.05	1.65E+03	0.51
BeO:Yb$_{0.01\%}$	1.25E+05	7.02	1.60	1.30E+04	162.67	2.05	1.71E+03	0.73
BeO:Er$_{0.01\%}$	1.86E+05	10.68	1.68	4.06E+04	52.77	2.05	1.50E+03	0.54
BeO:Gd$_{0.01\%}$	8.23E+04	9.70	1.54	2.79E+04	48.88	2.05	9.05E+02	0.74
BeO:Tb$_{0.01\%}$	1.51E+05	14.49	2.05	1.62E+04	68.91	2.05	1.07E+03	0.66
BeO:Tm$_{0.01\%}$	2.04E+05	6.89	1.59	9.10E+03	263.66	1.26	6.76E+03	0.60
BeO:Sm$_{0.01\%}$	2.12E+05	8.33	1.65	5.84E+03	191.09	1.05	5.62E+03	0.65
BeO:Pr$_{0.01\%}$	1.94E+05	9.39	1.61	5.21E+04	45.42	2.05	1.57E+03	0.61
BeO:Dy$_{0.01\%}$	1.67E+05	7.70	1.37	9.44E+04	37.24	2.05	1.86E+03	0.53

approximation of the actual situation. To learn more about the traps and transitions involved in OSL development, studies focused on the numerical solutions of the charge trafficking equations are required.

3.5. Effect of lanthanide co-doping in the luminescence of BeO:$Ce^{3+}_{0.01\%}$

According to the data obtained from single-lanthanide doped samples, the effect of another lanthanide co-doping on luminescence from the BeO:Ln^{3+} ceramic pellets was investigated. Although good progress has been observed in Ln^{3+} ion co-doped ceramic BeO, a comprehensive and full understanding of the TL and OSL mechanism originated from Ln^{3+} ions is still a major challenge. In this study, Ln^{3+} (Eu^{3+}, Nd^{3+}, Yb^{3+}, Er^{3+}, Gd^{3+}, Tb^{3+}, Tm^{3+}, Sm^{3+}, Pr^{3+} or Dy^{3+} as the co-dopants) effects on Ce^{3+} ions in host crystal were investigated. Although Eu^{3+} co-doped BeO:Ce^{3+} sample shows a relatively higher TL signal compared to the other samples (data not shown) (will be discussed later), only the results from some promising samples are presented here. Fig. 7. shows TL intensities from the BeO singly doped with Ce^{3+}, Er^{3+}, Tb^{3+}, Dy^{3+}, and BeO:Ce^{3+},Er^{3+}, BeO:Ce^{3+},Tb^{3+}, BeO:Ce^{3+},Dy^{3+} ceramics in linear and semi-log scale.

As is seen from Fig. 7, although TL glow curves BeO:Tb and BeO:Dy did not show the 350 °C TL peak, the TL glow curves from the BeO:Ce,Tb, and BeO:Ce,Dy samples showed this peak. It may be suggested that Ce^{3+} ions in BeO characterize the emission of the 350 °C TL peak. Furthermore, the TL glow curve shape of the BeO:Ce,Er possessed the same TL peaks of BeO:Er and BeO:Ce samples with changing intensities. One may conclude that the co-doped samples, in general, exhibited lower intensities than single-doped BeO samples (see Fig. 7). Similar to the decrease in TL intensities of the co-doped samples (Ce^{+}, Ln^{3+}), OSL efficiencies of them also behaved in the same decreasing tendency (data not shown). This may be originated from the decrease in the Ce^{3+} luminescence efficiency with temperature (i.e., thermal quenching) associated with the increase in possible non-radiative relaxation of the Ce^{3+} from the excited to the ground state [56]. The presence of a charge compensator in the lattice that would promote Ce^{3+} incorporation and cause emission appearing in the UV luminescence band can solve this quenching problem [9].

3.6. Effect of metal co-doping in the luminescence of BeO:$Ce_{0.01\%}$,$Ln^{3+}_{0.01\%}$

We also added the alkali metal ions to promote the luminescence sensitivity of the host material by creating more defects. In the literature, it has been shown that the Na^{+} co-doping can significantly improve the luminescence efficiency by acting as a probable charge compensator and increasing incorporation of the lanthanide dopants [12,13,57]. In one of our previous studies, the optimal concentration value for Na^{+} co-doping element, which significantly increased the luminescence emission, was found to be 5 mol% [13]. For this reason, a passive admixture (e.g., Na^{+} co-doping) was applied and Na^{+} content was kept constant at 5 mol% in this study.

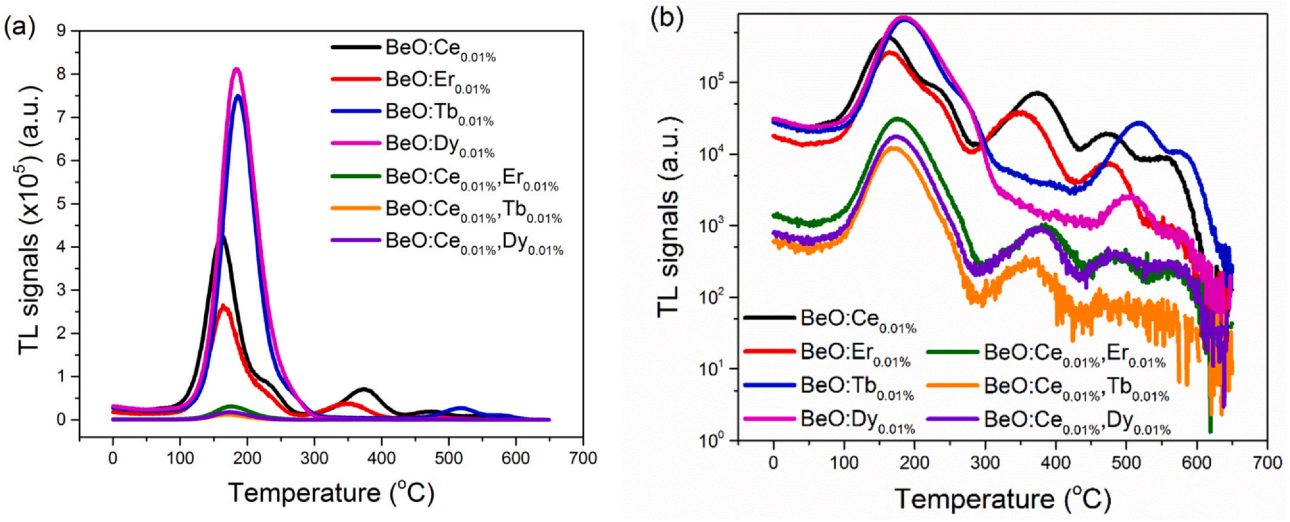

Fig. 7. TL glow curves of BeO ceramic pellets singly doped with Ce^{3+}, Er^{3+}, Tb^{3+}, Dy^{3+} and co-doped with Ln^{3+} (Ln^{3+} = Er^{3+}, Tb^{3+}, and Dy^{3+}); (a) in linear scale (b) in semi-log scale for better presentation of the high temperature peaks.

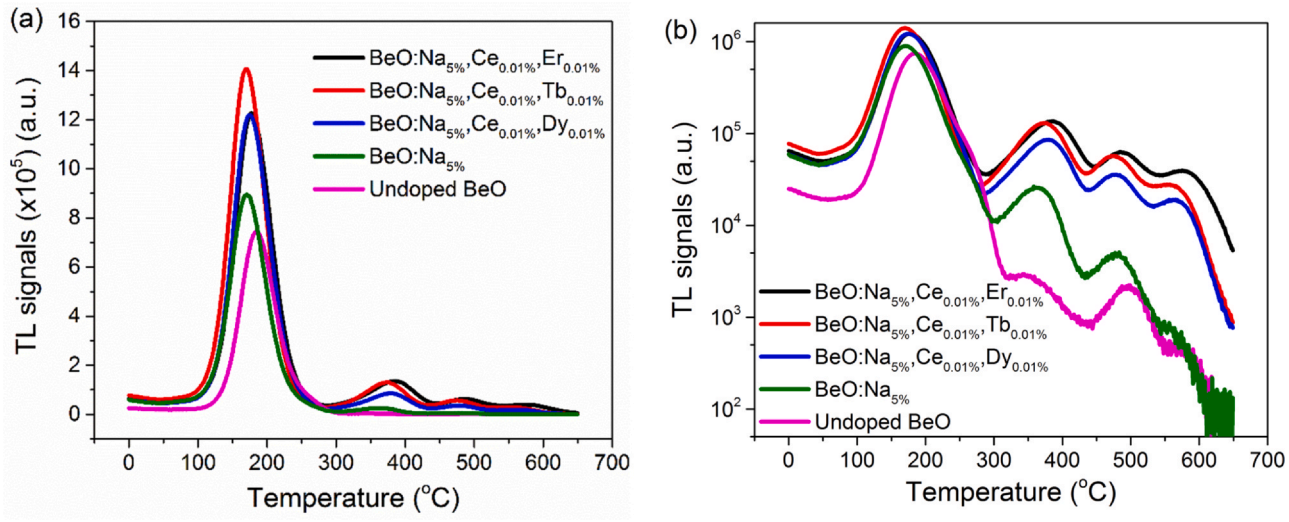

Fig. 8. TL glow curves of undoped BeO ceramic pellets, BeO doped with Ce^{3+} (0.01 mol%) and Er^{3+}, Tb^{3+}, Dy^{3+} at dopant concentration of 0.01 mol% and co-doped with Na^{+} (5 mol %); (a) in linear scale (b) in semi-log scale for the high temperature peaks to be depicted better.

To investigate the effect of Na^{+} co-doping on TL and OSL behaviors of BeO:$Ce_{0.01\%}$,$Ln_{0.01\%}$ ceramic pellets (Ln^{3+} = Eu^{3+}, Nd^{3+}, Yb^{3+}, Er^{3+}, Gd^{3+}, Tb^{3+}, Tm^{3+}, Sm^{3+}, Pr^{3+} or Dy^{3+}), TL glow curves, and OSL signals were obtained from the produced samples following 0.5 Gy dose exposure. Some of the TL and OSL curves from the promising samples, namely, BeO:$Na_{5\%}$,$Ce_{0.01\%}$,$Er_{0.01\%}$, BeO:$Na_{5\%}$,$Ce_{0.01\%}$,$Tb_{0.01\%}$, BeO:$Na_{5\%}$,$Ce_{0.01\%}$,$Dy_{0.01\%}$ and BeO:$Na_{5\%}$ were presented in Fig. 8 and Fig. 9, respectively. As can be seen from these figures, TL and OSL signal intensities were significantly increased by Na^{+} co-doping and even single Na^{+} doping. While no change occurred in the positions of the TL peaks, especially in the TL glow curves given in Fig. 8a, the intensities of the peaks located after 300 °C increased by two-factors when compared to that of the undoped BeO samples. Although single Na^{+} doping increased the characteristic TL signals, no change in the shape of TL glow curves was observed. These results proved that Na^{+} ion as a charge compensator in the lattice would promote Ce^{3+} incorporation and cause emission appearing in the UV luminescence band (will be discussed in Discussion). This causes an increase in luminescence efficiency. On the other hand, it can be said that OSL signals reach the background level (approximately 10^3 counts level) at longer stimulation times as compared with the OSL behavior of undoped sample, thus, in our measurements, an increase in lifetimes was observed for the BeO:$Na_{5\%}$,$Ce_{0.01\%}$,$Ln_{0.01\%}$ ceramic pellets (see Fig. 9). The relative total integrated TL and OSL intensities (the sum of the data from 0 up to 200 s) against the dopant elements were also examined. After Na^{+} co-doping there exists a 2-fold increase in both OSL and TL signal intensities (see Fig. A1 in Appendix A).

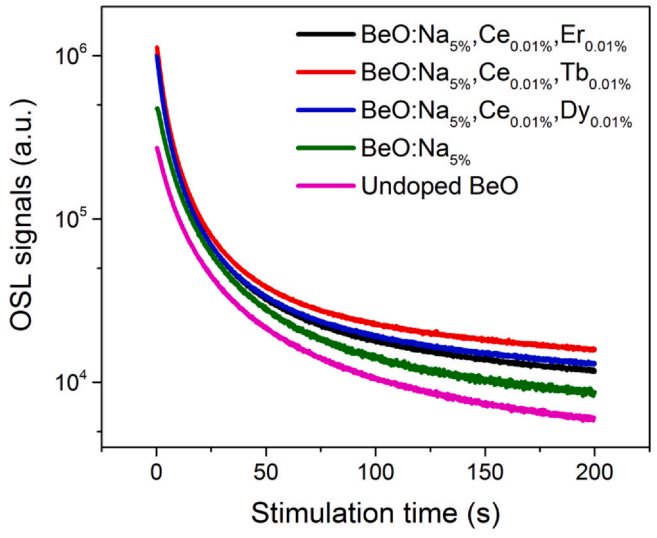

Fig. 9. OSL decay curves of undoped BeO ceramic pellets, BeO doped with Ce^{3+} (0.01 mol%) and Er^{3+}, Tb^{3+}, Dy^{3+} (0.01 mol%), and co-doped with Na^{+} (5 mol%).

Besides Na^{+}, other well-known alkali metals Li^{+} and K^{+} in the literature were also tested along with the lanthanides as co-dopants in this study. TL and OSL signals of Li- and K-co-doped samples (BeO:$Li_{5\%}$,$Ce_{0.01\%}$,$Er_{0.01\%}$, BeO:$Li_{5\%}$,$Ce_{0.005\%}$,$Tb_{0.05\%}$, BeO:$Li_{5\%}$,$Ce_{0.01\%}$,$Dy_{0.01\%}$ BeO:$K_{5\%}$,$Ce_{0.01\%}$,$Er_{0.01\%}$, BeO:$K_{5\%}$,$Ce_{0.005\%}$,$Tb_{0.05\%}$, and BeO:$K_{5\%}$,$Ce_{0.01\%}$,$Dy_{0.01\%}$ ceramic pellets) are presented in Fig. A2 of Appendix A Supplementary Data. The results showed that Na^{+} ions provided higher TL and OSL signals than Li^{+} and K^{+} ions. For this reason, Na^{+} ion was chosen as a better charge compensator in BeO structure and the study was continued with Na^{+} ion.

3.7. Concentration quenching study

To investigate the effect of dopant concentration quenching on TL and OSL intensities of Ln^{3+}-doped BeO ceramics and to determine the optimal concentration for achieving highest luminescent sensitivity, TL and OSL readouts of BeO with various $Na_{5\%}$,$Ce_{x\%}$,$Er_{x\%}$; $Na_{5\%}$,$Ce_{x\%}$,$Tb_{x\%}$, and $Na_{5\%}$,$Ce_{x\%}$,$Dy_{x\%}$ concentrations (x = 0.001, 0.005, 0.01, 0.05, 0.1 mol%) were performed after 0.5 Gy beta dose exposure. Fig. 10 shows the change in TL and OSL intensities of BeO:-$Na_{5\%}$,$Ce_{0.01\%}$,$Er_{x\%}$, BeO:$Na_{5\%}$,$Ce_{0.01\%}$,$Tb_{x\%}$, and BeO:$Na_{5\%}$,$Ce_{0.01\%}$,$Dy_{x\%}$ ceramic pellets produced at concentrations given above. First, the Er^{3+}, Tb^{3+} and Dy^{3+} concentrations were changed by keeping the concentrations of Na^{+} and Ce^{3+} ions constant as 5 mol% and 0.01 mol %, respectively. With varying dopant concentrations, TL and OSL intensities showed similar concentration quenching behavior (see Fig. 10a and b). While the optimal Tb concentration value for BeO:-$Na_{5\%}$,$Ce_{0.01\%}$,$Tb_{x\%}$sample was determined to be as 0.05 mol%, and the highest TL and OSL intensities were obtained at 0.01 mol% Er and Dy concentrations for BeO:$Na_{5\%}$,$Ce_{0.01\%}$,$Er_{x\%}$, and BeO:$Na_{5\%}$,$Ce_{0.01\%}$,$Dy_{x\%}$ samples. On the other hand, with varying Ce^{3+} concentration, the maximum TL and OSL intensities were obtained from the combined measurements of the BeO:$Na_{5\%}$,$Ce_{0.01\%}$,$Er_{0.01\%}$; BeO:-$Na_{5\%}$,$Ce_{0.005\%}$,$Tb_{0.05\%}$ and BeO:$Na_{5\%}$,$Ce_{0.01\%}$,$Dy_{0.01\%}$ ceramic pellets (see Fig. 11a and b). The TL and OSL intensities have a great dependence on Ln^{3+} dopant concentration. The luminescence increases

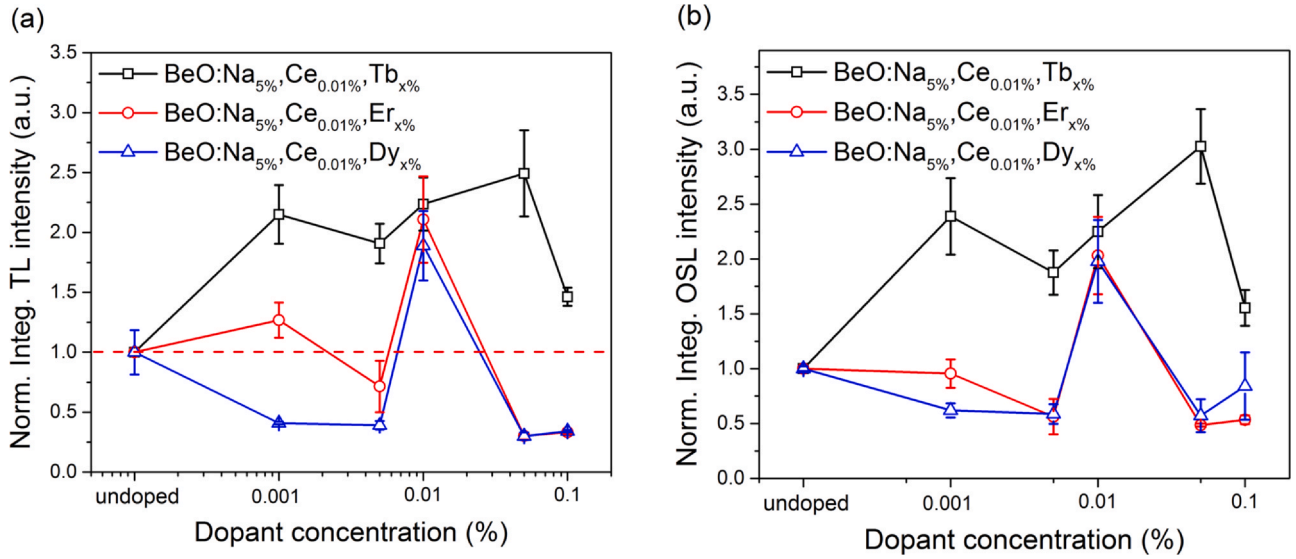

Fig. 10. The changes in normalized integrated (a) TL intensities; (b) OSL intensities of BeO:$Na_{5\%}$,$Ce_{0.01\%}$,$Er_{x\%}$; BeO:$Na_{5\%}$,$Ce_{0.01\%}$,$Tb_{x\%}$, and BeO:$Na_{5\%}$,$Ce_{0.01\%}$,$Dy_{x\%}$ ceramic pellet samples prepared with various concentrations (x = 0.001, 0.005, 0.01, 0.05, 0.1 mol%) when compared with the TL and OSL intensities of undoped BeO samples in semi-log scale. The error bars show the experimental standard deviations of mean values from three samples in each readout.

with Ln^{3+} concentration to a certain extent, above this point, the luminescence begins to decrease, due to parity or aggregation of Ln^{3+} atoms at a high concentration which leads to efficient resonant energy transfer between Ln^{3+}/Na^{+} ions and a fraction of energy migration to distant quenchers, then quenching behavior appears as a result [58].

In this study, increased luminescence efficiency in desired emission regions and controlled luminescence signals obtained with lanthanide doping on purpose are important for the dosimetric potential of the materials. The minimum detectable dose values were calculated to test the advantage of the three newly developed dosimetric materials over the undoped BeO. MDD values were evaluated by 3σ with 99.73% confidence level as 1.2 ± 0.3 mGy, 721 ± 17 μGy, 271 ± 5 μGy, 554 ± 10 μGy for undoped BeO, BeO:$Na_{5\%}$,$Ce_{0.005\%}$,$Tb_{0.05\%}$, BeO:$Na_{5\%}$,$Ce_{0.01\%}$,$Er_{0.01\%}$, and BeO:$Na_{5\%}$,$Ce_{0.01\%}$,$Dy_{0.01\%}$ ceramic pellets, respectively.

On the other hand, to test whether the charge population in traps is stable or not, after 0.5 Gy beta doses fading characteristics of newly developed BeO ceramics were investigated in three days. It was observed that almost 94% of the OSL signals remained stable after 3 days. We found the fading of around 87% when the undoped BeO was read out at about 3 days after irradiation. This behavior is of course extremely important in the practical use of these materials for dosimetric applications. These results suggest that the OSL and TL intensities of three newly developed BeO pellets (BeO:$Na_{5\%}$,$Ce_{0.01\%}$,$Er_{0.01\%}$; BeO:$Na_{5\%}$,$Ce_{0.005\%}$,$Tb_{0.05\%}$ and BeO:$Na_{5\%}$,$Ce_{0.01\%}$,$Dy_{0.01\%}$) are found to be highly sensitive to radiation with superior dosimetric properties.

4. Discussion

The luminescence mechanism of Ln^{3+} ions is known depending on their location in the host lattice. If the Ln^{3+} ions have similar chemical properties with host materials, such as the same oxidation state and similar ionic radius, it is easy to include Ln^{3+} ions in the

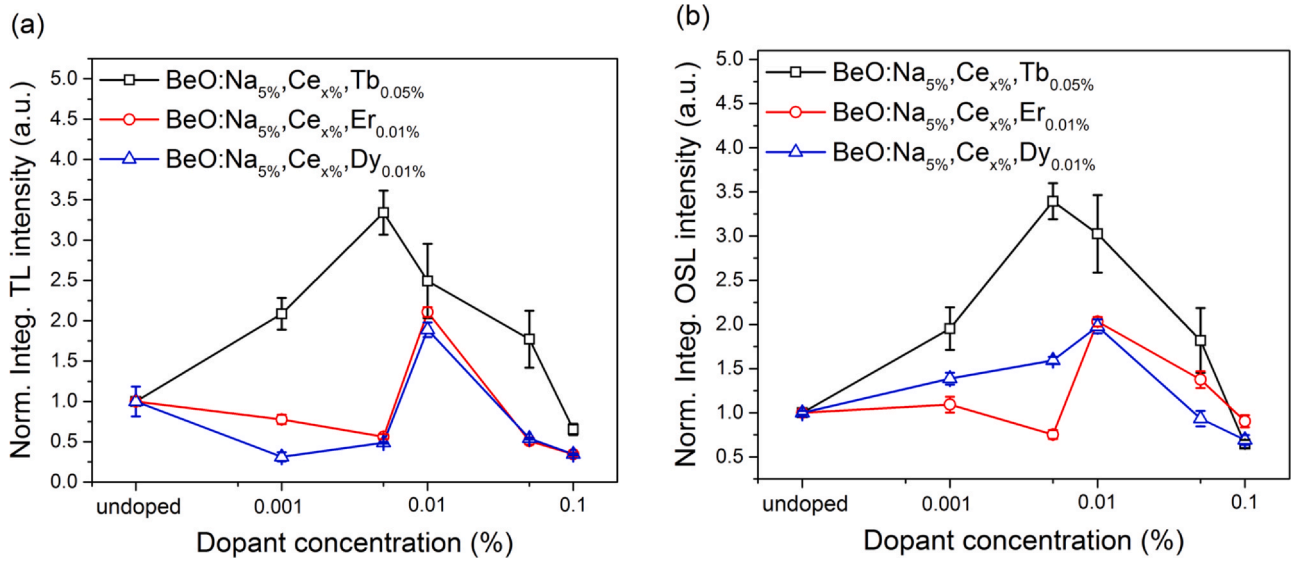

Fig. 11. The changes in normalized integrated (a) TL intensities; (b) OSL intensities of BeO:$Na_{5\%}$,$Ce_{x\%}$,$Er_{0.01\%}$; BeO:$Na_{5\%}$,$Ce_{x\%}$,$Tb_{0.05\%}$, and BeO:$Na_{5\%}$,$Ce_{x\%}$,$Dy_{0.01\%}$ ceramic pellet samples prepared with different concentrations (x = 0.001, 0.005, 0.01, 0.05, 0.1 mol%) when compared with the TL and OSL intensities of undoped BeO samples in semi-log scale. The error bars show the experimental standard deviations of mean values from three samples in each readout.

host lattice in place of host metal ions. Here, due to the remarkable differences between the ionic radius of Ln^{3+} and Be^{2+}, it would create some local distortion that may stabilize holes from the valance band [59]. In such a case, it can be expected that even a small distortion may lead to an increase or decrease in luminescence efficiency. To determine the effect of Ln^{3+} on the BeO lattice and how the luminescence mechanism exists, the results for single-doped, co-doped, and metal-doped BeO ceramics presented here must be discussed from the spectroscopic properties of underlying Ln^{3+} ions.

Fig. 12. shows the OSL emission spectra of Ln^{3+}-doped BeO ceramics following the 300 Gy beta dose through a transmission range of the Hoya U-340 filter which used in the RisØ reader. As is seen from the figure that the main OSL emission bands are located between ~300 and ~360 nm; the first being the dominant band. These results showed that the dominant luminescence bands in RL and OSL processes might be different. However, luminescence bands located between 300 and 400 nm (i.e., 3–4 eV) are dependent on the same luminescence mechanism in both cases which have been observable using U-340 filter. When the OSL emissions of single Ln^{3+}-doped BeO samples were compared with the emission obtained from the undoped sample, it was observed that some single Ln^{3+}ions shifted the dominant luminescence band towards higher wavelengths in the BeO structure (see Fig. 12a). Moreover, only an increase in the emissions of Ce^{3+}, Er^{3+}, Tb^{3+}, Gd^{3+}, Pr^{3+} and Dy^{3+} doped samples was observed. With the Ln^{3+} co-doping, a reduction in OSL emission was observed here as well, while an increase in emissions after 360 nm was observed (see Fig. 12b). With the addition of Na^{+} ion to the structure, OSL emissions have increased significantly recorded through the Hoya U-340 filter.

When we examined the results of TL and OSL obtained from single Ln^{3+} doped BeO samples more closely, a decrease in luminescence efficiency was observed with increasing Ln^{3+} concentration, similar to RL emissions. Concentration quenching, which can be regarded as a non-radiative process, is one of the main things to avoid when optimizing additive concentration. The decrease in luminescence, which was observed as a result of the increasing Ln^{3+} concentration in the structures with rich energy levels (general activators such as Tb^{3+}, Er^{3+}, Tm^{3+}, Pr^{3+}), is the concentration-dependent cross-relaxation (CR) affecting the non-radiative transition population of stimulated Ln^{3+} ions [33].

Fig. 5 shows that the Ce^{3+} ion increases the luminescence sensitivity of the BeO host material by affecting the trap region corresponding to the TL peaks responsible for the OSL signals. Besides, the fact that the Ce^{3+} ion is a good sensitizer that can transfer energy to the activators around in a possible situation has encouraged us to obtain a BeO:Ce^{3+} based "host + sensitizer + activator" type luminescent material. Energy transfer for ions plays an important role in luminescent materials. Energy transfer from the sensitizer to the activator can be achieved by the spectral overlap of the emission spectrum of the sensitizer ion and the absorption spectrum of the activator ion [60]. The reason why the Eu^{3+} co-doped BeO:Ce^{3+} sample shows a relatively higher TL signal compared to the other samples is the existence of a wide emission band of Ce^{3+} ion, approximately at 330–420 nm related with the transition from 5d level to $^2F_{5/2} \rightarrow {}^2F_{7/2}$ levels and its overlapping with the absorption band of Eu^{3+} ion represented by the transition from $^7F_0 \rightarrow {}^5L_6$ [60]. In this study, the Er^{3+} co-doped BeO:Ce^{3+} sample showed the highest OSL signals. It was concluded that a passive admixture (charge compensator) ion such as Na^{+} is needed to facilitate energy transfer between Ln^{3+} ions in the "host (BeO) + sensitizer (Ce^{3+}) + activator (such as Tb^{3+}, Tm^{3+}, Dy^{3+}, Nd^{3+})" type samples, that is, to increase the UC quantum yield and consequently to improve luminescence.

Apparently, Na^{+} plays several roles, including charge compensation and possibly lattice stress relief on Ln^{3+} doped BeO. It was observed in Fig. 8 that TL and OSL efficiencies obtained from the BeO:Ce^{3+},Ln^{3+} samples increased almost 2 times after Na^{+} co-doping.

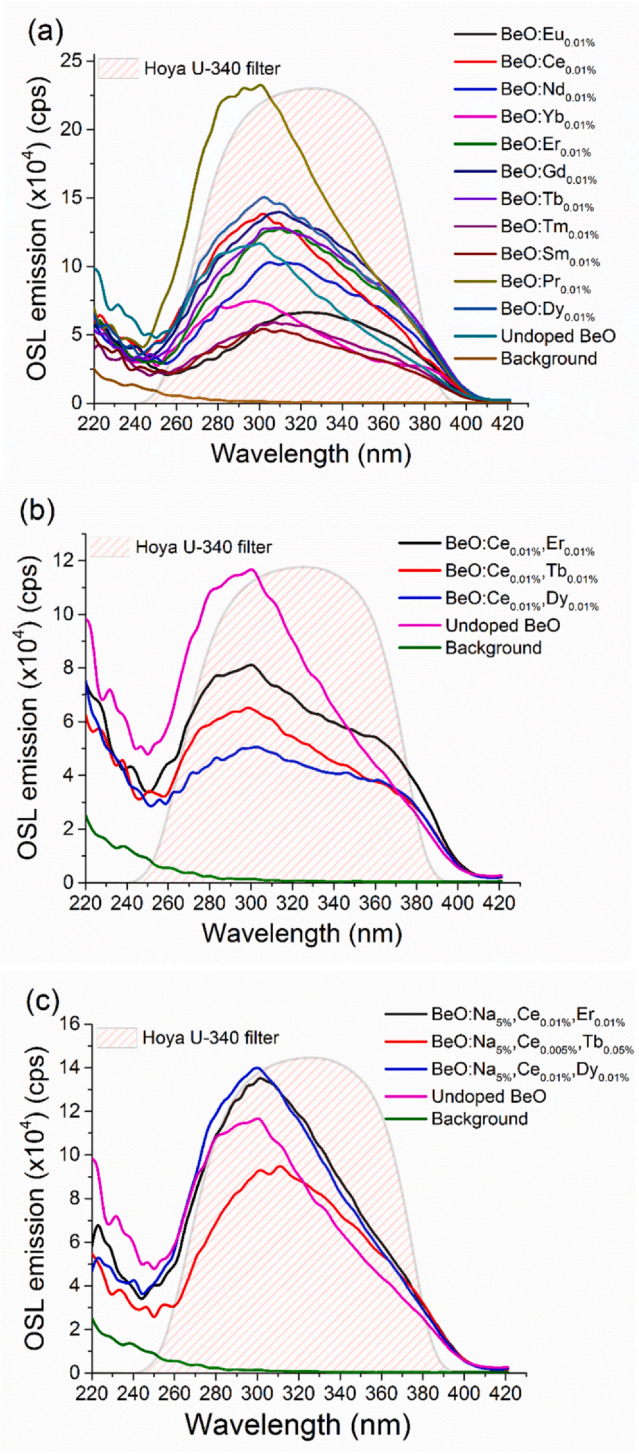

Fig. 12. OSL emission spectra of previously irradiated BeO ceramics with 300 Gy beta dose and using 475 nm excitation; (a) for the single Ln^{3+}-doped BeO; (b) for the Ln^{3+} doped and co-doped BeO, (c) after adding the alkali metal ions Na^{+} as co-dopants to BeO host oxides. The excitation monochromator was 475 nm, and the emission spectra were scanned from 240 to 420 nm in 3 nm increments using 0.1 s integration time. The excitation time was 60 s. All the OSL emission spectra presented here were previously corrected by the spectral response of the system.

Herein, the reason for the remarkable increase in luminescence might be due to Na^{+} ions acting as a charge compensator and causing an increase in UC quantum yield and consequently an energy transfer between the emission centers introduced by Na^{+} and the Ln^{3+} dopants. The energy transfer mentioned here, most probably takes place effectively if the condition of energy resonance and

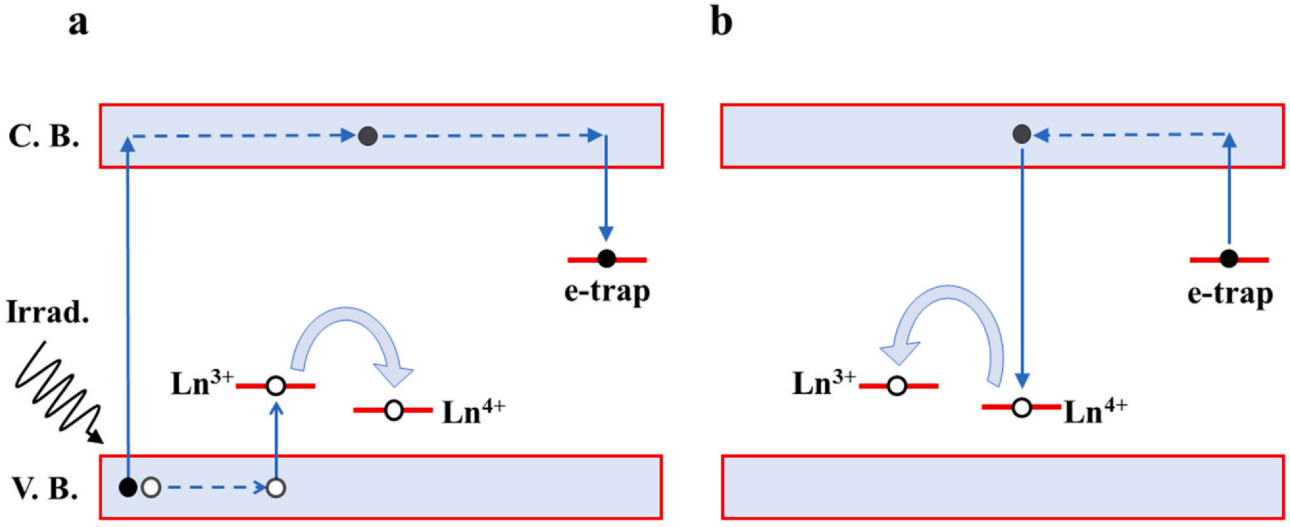

Fig. 13. Proposed TL/OSL mechanism: (a) During irradiation, charge carriers (electron and holes) are created, and trapped by electron-traps and hole-traps (Ce^{3+}, Pr^{3+}, Tb^{3+}), ($Ln^{3+} + h^{+} \rightarrow Ln^{4+}$). (b) During TL/OSL readout (thermal or optical stimulation), electrons are released from trapping centers (Sm^{3+}, Eu^{3+}, Yb^{3+}, Dy^{3+}, Er^{3+}) and recombine with Ln^{4+} ions (Ce^{4+}, Pr^{4+}, Tb^{4+}), converting them to Ln^{3+} in an excited state. Luminescence occurs with the relaxation of these compounds. Electrons and holes are represented by solid and open circles, respectively.

spatial proximity between the involved centers are satisfied. This will be met due to a high Na^{+} concentration in the structure [61]. As is seen in Fig. 12c, the broadening UV emission bands mean that they likely match the resonance condition for most of the sensitizers (here specifically Ce^{3+}) or other activators, Ln^{3+} (here specifically Er^{3+}, Tb^{3+}, Dy^{3+}). On the other hand, regarding the role of Na^{+} dopant in BeO, it is clear to say that a negative effective charge defect $(Na_{Be})^{-}$ occurs with the Na^{+} substitution for Be^{2+}. This negative charge defect may compensate for the positive effective charge defect $(Ln_{Be})^{+}$ occurring with the Ln^{3+} substituting for Be^{2+}. As a hypothesis, the assumption that the ideal substitution of Na^{+} for Be^{2+} needs evidence. One can expect, e.g., an interstitial charge-neutralized by OH-. Negative charge $(Na_{Be})^{-}$ defects may compensate for the incorporation of positive effective charge in an intrinsic defect of BeO crystal [10,13,62]. As a result of XRD analyzes, a decrease in oxygen vacancies which are capable of improving luminescence in the structure was observed with Ln^{3+} doping. The $(Na_{Be})^{-}$ defects obtained by Na^{+} co-doping, just like oxygen vacancies, cause crystal field distortion and might act as compensators for the energy transfer from host to Ln^{3+} ion due to the strong mixing of charge transfer states and enhances the luminescence intensity [58,63]. In this work, considering this compensation effect, differences in ionic radius and changes in crystal field energy can be considered to cause a significant increase in luminescence signals. The roles of Na^{+} as a dopant contributing to the enhancement of luminescence and improving dosimetric characteristics of BeO ceramic pellets were presented elsewhere in the literature [12,13,57,64].

Considering both TL and OSL signals presented in Fig. 8, the most sensitive examples were selected as BeO:Na,Ce,Er; BeO:Na,Ce,Tb, and BeO:Na,Ce,Dy. Optimizing the concentration of optically active ions is potentially the easiest way to improve the UC quantum yield. Therefore, in this study, the concentrations of Ln^{3+} ions contained in "host + sensitizer + activator" type of final products were optimized as the BeO:$Na_{5\%}$,$Ce_{0.01\%}$,$Er_{0.01\%}$, BeO:$Na_{5\%}$,$Ce_{0.005\%}$,$Tb_{0.05\%}$, and BeO:-$Na_{5\%}$,$Ce_{0.01\%}$,$Dy_{0.01\%}$. The source of the enhanced luminescence obtained here, besides the concentration optimization, can be the strong energy transfer between Ln^{3+} ions. The energy transfer process simply begins by getting excite the electrons located at $^{2}F_{5/2}$ ground state of Ce^{3+} ions to the 5d excited level. While some electrons return to the ground states of Ce^{3+} ions by exhibiting UV-blue emissions, some electrons transfer to the acceptor levels e.g., $^{5}D_{4}$ excited state of Tb^{3+} ions and higher energy levels of Dy^{3+} ions. As a result of the return of electrons to the ground state energy levels of activator ions, characteristic visible region emissions (blue light and yellow light emissions of Dy^{3+} ions, green emissions of Er^{3+}, and Tb^{3+} ions) of activator ions may be observed. A more detailed energy transfer mechanism in Ln^{3+} ions was discussed in the literature [60].

Of course, a TL/OSL model is still required to represent the existing complex luminescence process. It is clear to say that trivalent lanthanides in BeO lattice should establish energy levels in the forbidden band and show themselves actively in recombination processes. The Ln^{3+} can act as electron traps or hole traps, depending on their location concerning the delocalized energy bands and the Fermi level. In this study, the luminescence process simply begins by creating charge carriers as a result of irradiating the crystal as illustrated in Fig. 13. The electrons and holes move freely inside the crystal and are trapped at defects. Considering the general theory of defects [65], and the behavior of the trivalent lanthanide impurities (Ln^{3+}) in various types of phosphors (e.g. YPO_4 and CaF_2 [59,66]), in our samples, Ce^{3+}, Pr^{3+}, and Tb^{3+} may act as hole traps and become quadrivalent ions (Ce^{4+}, Pr^{4+}, Tb^{4+}) during irradiation. With heat or light stimulation, trapped electrons are escaped from the electron traps (Sm^{3+}, Eu^{3+}, Yb^{3+}, Dy^{3+}, Er^{3+}). As a result of the recombination of these released electrons with Ln^{4+} ions, Ln^{3+} ions occur in excited states. After the relaxation of Ln^{3+} ions, they decay to the ground states, and simultaneous emission of the photons i.e. luminescence is observed (see Fig. 13). More detailed studies on the role of lanthanides in BeO ceramic pellets such as temperature dependence of RL signals and TL emissions are necessary to confirm the proposed luminescence mechanism.

5. Conclusion

In this work, the successful incorporation of Ln^{3+} and Na^{+} alkali ions into the lattice of BeO ceramic was achieved using the conventional co-precipitation method. It was investigated that co-doping of BeO with impurities such as Ln^{3+} ions abovementioned is an effective way to enhance luminescence efficiency. In our experiments, the incorporated impurity Ce^{3+} served as a sensitizer. Besides Ce^{3+} ions, other impurities like Er^{3+}, Tb^{3+}, and Dy^{3+}ions participated in energy transfer within the matrix. We revealed a luminescence mechanism based on beryllium sublattice-mediated energy migration, which facilitates efficient upconversion emissions from a series of Ln^{3+} ions (Er^{3+}, Tb^{3+} and Dy^{3+}) without intermediary energy levels.

Contrary to Ln^{3+} ions, alkali ions, intentionally incorporated into Ln^{3+} doped BeO did not directly participate in the optical process (e.g., energy transfer) within the hosts, but were capable of enhancing upconversion efficiency as well. OSL emission intensities of the BeO:Ce^{3+},Ln^{3+} (Ln= Er^{3+}, Tb^{3+} and Dy^{3+}) co-doped with 5% mol Na^{1+} ions were enhanced by about 2 times. Such improvement could be attributed to charge compensation with Na^{+} ions because the $(Na_{Be})^{-}$ defects locating around the Ln^{3+} ions cause the strong mixing of charge-transfer states.

We investigated the luminescence characteristics of the Ln^{3+} and Na^{+} doped BeO ceramic pellets using RL, TL, and OSL techniques. The XRD patterns and Raman spectra showed that Ln^{3+} ions were incorporated into the BeO lattice and might be suggested as substituting for Be^{2+} lattice sites rather than locating in interstitial positions. All the Ln^{3+} doped BeO ceramic samples exhibited their typical RL emissions along with the characteristic RL emission of BeO ranging between 200 and 450 nm. With increasing Ln^{3+} concentration, there was a significant decrease in TL and OSL signals due to parity or aggregation of Ln^{3+} atoms at high concentrations. The luminescence mechanism model in BeO is complex. It can be suggested that the recombination process in BeO might be improved by adding suitable Ln^{3+} dopants. In this work, a model was also proposed to explain the basic luminescence properties of Ln^{3+} doped BeO ceramics.

These results strongly suggest that the newly developed three ceramic pellets BeO:$Na_{5\%}$,$Ce_{0.01\%}$,$Er_{0.01\%}$; BeO:$Na_{5\%}$,$Ce_{0.005\%}$,$Tb_{0.05\%}$ and BeO:$Na_{5\%}$,$Ce_{0.01\%}$,$Dy_{0.01\%}$ performed the high OSL and TL intensities. In the future, the aforementioned ceramics with these outstanding Ln^{3+} and Na^{+} dopants will be tested and involved in several comparison studies with the commercial dosimeters.

CRediT authorship contribution statement

Volkan ALTUNAL: Conceptualization, Methodology, Validation, Formal analysis, Investigation, Writing - original draft, Visualization. **Veysi GUCKAN:** Conceptualization, Methodology, Investigation. **Adnan OZDEMIR:** Visualization, Investigation. **Ahmet EKICIBIL:** Methodology, Investigation, Writing - review & editing. **Faruk KARADAG:** Visualization, Investigation, Writing - review & editing. **İlhami YEGINGIL:** Resources, Writing - review & editing. **Y. ZYDHACHEVSKYY:** Investigation, Methodology. **Zehra YEGINGIL:** Conceptualization, Writing - review & editing, Visualization, Project administration, Funding acquisition, Supervision.

Declaration of Competing Interest

The authors declare that they have no known competing financial interests or personal relationships that could have appeared to influence the work reported in this paper.

Acknowledgments

This work was supported by the NATO SPS MYP program, Belgium under project number G5647 and Cukurova University Research Projects Development and Coordination Unit, Turkey under the project numbers FDK-2018-10190, FAY-2019-11571, and FAY-2020-12932, FBA-2020-13126. The authors thank NATO and Cukurova University for supporting this research. We are grateful to Prof. Kasım Kurt and Tayfun Cavdar from Mersin University for RL emission measurements.

Appendix A. Supporting information

Supplementary data associated with this article can be found in the online version at doi:10.1016/j.jallcom.2021.160105.

References

[1] T. Kron, Applications of thermoluminescence dosimetry in medicine, Radiat. Prot. Dosim. 85 (1999) 333–340.
[2] S.W. McKeever, Thermoluminescence of Solids, Cambridge University Press, 1988.
[3] E.G. Yukihara, S.W. McKeever, Optically Stimulated Luminescence: Fundamentals and Applications, John Wiley & Sons, 2011.
[4] I. IEC, 62304: 2006 Medical device software–software life cycle processes, International Electrotechnical Commission, Geneva, (2006).
[5] Y.S. Horowitz, Thermoluminescence and thermoluminescent dosimetry, v. 2, (1984).
[6] T. Berger, M. Hajek, TL-efficiency—overview and experimental results over the years, Radiat. Meas. 43 (2008) 146–156.
[7] I. IAEA, Safety Glossary Terminology Used in Nuclear Safety and Radiation Protection 2007 Edition, IAEA, Vienna, (2007).
[8] S. Bastani, L. Oliveira, E. Yukihara, Development and characterization of lanthanide-doped $CaSO_4$ for temperature sensing applications, Opt. Mater. 92 (2019) 273–283.
[9] L.C. Oliveira, E.G. Yukihara, O. Baffa, MgO:Li,Ce,Sm as a high-sensitivity material for Optically Stimulated Luminescence dosimetry, Sci. Rep. 6 (2016) 24348.
[10] E.G. Yukihara, E.D. Milliken, L.C. Oliveira, V.R. Orante-Barrón, L.G. Jacobsohn, M.W. Blair, Systematic development of new thermoluminescence and optically stimulated luminescence materials, J. Lumin. 133 (2013) 203–210.
[11] V. Altunal, V. Guckan, A. Ozdemir, N. Can, Z. Yegingil, Luminescence characteristics of Al-and Ca-doped BeO obtained via a sol-gel method, J. Phys. Chem. Solids 131 (2019) 230–242.
[12] V. Altunal, V. Guckan, A. Ozdemir, Z. Yegingil, Radiation dosimeter utilizing optically stimulated luminescence of BeO:Na,Tb,Gd ceramics, J. Alloy. Compd. 817 (2020) 152809.
[13] V. Altunal, V. Guckan, Y. Yu, A. Dicker, Z. Yegingil, A newly developed OSL dosimeter based on beryllium oxide: BeO:Na,Dy,Er, J. Lumin. 222 (2020) 117140.
[14] V. Guckan, V. Altunal, N. Nur, T. Depci, A. Ozdemir, K. Kurt, Y. Yu, I. Yegingil, Z. Yegingil, Studying $CaSO_4$:Eu as an OSL phosphor, Nucl. Instrum. Methods Phys. Res. Sect. B Beam Interact. Mater. At. 407 (2017) 145–154.
[15] V. Guckan, V. Altunal, A. Ozdemir, Z. Yegingil, Optically stimulated luminescence of MgO:Na,Li phosphor prepared using solution combustion method, J. Alloy. Compd. 835 (2020) 155253.
[16] V. Guckan, A. Ozdemir, V. Altunal, I. Yegingil, Z. Yegingil, Studies of blue light induced phototransferred thermoluminescence in $CaSO_4$:Mg, Nucl. Instrum. Methods Phys. Res. Sect. B Beam Interact. Mater. At. 448 (2019) 31–38.
[17] A. Ozdemir, V. Altunal, K. Kurt, T. Depci, Y. Yu, Y. Lawrence, N. Nur, V. Guckan, Z. Yegingil, Thermoluminescence properties of $Li_2B_4O_7$:Cu, B phosphor synthesized using solution combustion technique, Radiat. Phys. Chem. 141 (2017) 352–362.
[18] A. Ozdemir, G.S. Polymeris, E. Şahiner, E. Aşlar, V. Guckan, V. Altunal, N. Meriç, Z. Yegingil, Evaluation of thermoluminescence trapping parameters in $Li_2B_4O_7$ co-doped with Ag^{+} and Gd^{3+} using various experimental techniques, Nucl. Instrum. Methods Phys. Res. Sect. B Beam Interact. Mater. At. 461 (2019) 70–76.
[19] S. Watanabe, T.K. Gundu Rao, P.S. Page, B.C. Bhatt, TL, OSL and ESR studies on beryllium oxide, J. Lumin. 130 (2010) 2146–2152.
[20] V. Altunal, V. Guckan, A. Ozdemir, A. Sotelo, Z. Yegingil, Effect of sintering temperature on dosimetric properties of BeO ceramic pellets synthesized using precipitation method, Nucl. Instrum. Methods Phys. Res. Sect. B Beam Interact. Mater. At. 441 (2019) 46–55.
[21] S.W. McKeever, M. Moscovitch, P.D. Townsend, Thermoluminescence dosimetry materials: properties and uses, (1995).
[22] C.R. Rhyner, W.G. Miller, Radiation dosimetry by optically-stimulated luminescence of BeO, Health Phys. 18 (1970) 681–684.
[23] E. Bulur, H.Y. Goksu, OSL from BEO ceramics: new observations from an old material, Radiat. Meas. 29 (1998) 639–650.
[24] A. Jahn, M. Sommer, W. Ullrich, M. Wickert, J. Henniger, The BeOmax system – dosimetry using OSL of BeO for several applications, Radiat. Meas. 56 (2013) 324–327.
[25] M. Sommer, J. Henniger, Investigation of a BeO-based optically stimulated luminescence dosemeter, Radiat. Prot. Dosim. 119 (2006) 394–397.
[26] M. Sommer, A. Jahn, J. Henniger, Beryllium oxide as optically stimulated luminescence dosimeter, Radiat. Meas. 43 (2008) 353–356.
[27] M. Sommer, A. Jahn, J. Henniger, A new personal dosimetry system for HP(10) and HP(0.07) photon dose based on OSL-dosimetry of beryllium oxide, Radiat. Meas. 46 (2011) 1818–1821.
[28] A. Jahn, M. Sommer, J. Henniger, OSL efficiency for BeO OSL dosimeters, Radiat. Meas. 71 (2014) 104–107.
[29] D.R. Vij, N. Singh, Thermoluminescence dosimetric properties of beryllium oxide, J. Mater. Sci. 32 (1997) 2791–2796.
[30] L. Bøtter-Jensen, S.W. McKeever, A.G. Wintle, Optically Stimulated Luminescence Dosimetry, Elsevier, 2003.
[31] V. Altunal, V. Guckan, A. Ozdemir, Z. Yegingil, A calcination study on BeO ceramics for radiation dosimetry, Mater. Res. Bull. 130 (2020) 110921.
[32] V. Altunal, Z. Yegingil, T. Tuken, T. Depci, A. Ozdemir, V. Guckan, N. Nur, K. Kurt, E. Bulur, Optically stimulated luminescence characteristics of BeO nanoparticles synthesized by sol-gel method, Radiat. Meas. 118 (2018) 54–66.
[33] X. Chen, Y. Liu, D. Tu, Lanthanide-Doped Luminescent Nanomaterials, Springer, 2016.

[34] D.R. Gamelin, H.U. Güdel, Design of luminescent inorganic materials: new photophysical processes studied by optical spectroscopy, Acc. Chem. Res. 33 (2000) 235–242.
[35] F. Auzel, Upconversion and anti-stokes processes with f and d ions in solids, Chem. Rev. 104 (2004) 139–174.
[36] D. Yang, Z. Hou, Z. Cheng, C. Li, J. Lin, Current advances in lanthanide ion (Ln 3+)-based upconversion nanomaterials for drug delivery, Chem. Soc. Rev. 44 (2015) 1416–1448.
[37] C. Chen, C. Li, Z. Shi, Current advances in lanthanide-doped upconversion nanostructures for detection and bioapplication, Adv. Sci. 3 (2016) 1600029.
[38] V. Altunal, V. Guckan, Y. Yu, A. Dicker, Z. Yegingil, A newly developed OSL dosimeter based on beryllium oxide: BeO: Na, Dy, Er, J. Lumin. 222 (2020) 117140.
[39] O. Bilgili, The effects of Mn doping on the structural and optical properties of ZnO, Acta Phys. Pol. A 136 (2019) 460–466.
[40] C. Lorbeer, F. Behrends, J. Cybinska, H. Eckert, A.-V. Mudring, Charge compensation in RE 3+(RE= Eu, Gd) and M+(M= Li, Na, K) co-doped alkaline earth nanofluorides obtained by microwave reaction with reactive ionic liquids leading to improved optical properties, J. Mater. Chem. C 2 (2014) 9439–9450.
[41] M.S. Norazlina, S. Shanmugan, D. Mutharasu, Structural analysis of BeO nanoparticles synthesized by polyacrylamide gel route, Adv. Sci. Focus 1 (2013) 362–366.
[42] M. Moram, M. Kappers, F. Massabuau, R. Oliver, C. Humphreys, The effects of Si doping on dislocation movement and tensile stress in GaN films, J. Appl. Phys. 109 (2011) 073509.
[43] T. Theivasanthi, M. Alagar, Electrolytic synthesis and characterizations of silver nanopowder, arXiv preprint arXiv:1111.0260, (2011).
[44] U.D. Wdowik, Structural stability and thermal properties of BeO from the quasiharmonic approximation, J. Phys. Condens Matter 22 (2010) 045404.
[45] S.M. Lee, Y. Jang, J. Jung, J.H. Yum, E.S. Larsen, C.W. Bielawski, W. Wang, J.-H. Ryou, H.-S. Kim, H.-Y. Cha, Atomic-layer deposition of crystalline BeO on SiC, Appl. Surf. Sci. 469 (2019) 634–640.
[46] I.N. Ogorodnikov, V.Y. Ivanov, A.V. Kruzhalov, Short-wavelenght luminescence and thermostimulated processes in single crystals of BeO, Radiat. Meas. 24 (1995) 417–421.
[47] I. Ogorodnikov, A. Kruzhalov, Defect properties of beryllium oxide, Materials Science Forum, Trans Tech Publ, 1997, pp. 51–56.
[48] E.G. Yukihara, Luminescence properties of BeO optically stimulated luminescence (OSL) detectors, Radiat. Meas. 46 (2011) 580–587.
[49] J.-C.G. Bünzli, S.V. Eliseeva, Basics of lanthanide photophysics, Lanthanide Luminescence, Springer, 2010, pp. 1–45.
[50] X. Zeng, J. Yuan, L. Zhang, Synthesis and photoluminescent properties of rare earth doped ZnO hierarchical microspheres, J. Phys. Chem. C 112 (2008) 3503–3508.
[51] L. Hobzova, Improved band model of BeO ceramics, Phys. Status Solidi A Appl. Res. 60 (1980) K207–K209.
[52] R. Chen, S.W. McKeever, Theory of Thermoluminescence and Related Phenomena, World Scientific, 1997.
[53] J.T. Randall, M.H.F. Wilkins, Phosphorescence and electron traps-I. The study of trap distributions, Proceedings of the Royal Society of London. Series A. Mathematical and Physical Sciences, 184, (1945) 365–389.
[54] G. Garlick, A. Gibson, The electron trap mechanism of luminescence in sulphide and silicate phosphors, Proc. Phys. Soc 60 (1948) 574 (1926–1948).
[55] S. McKeever, R. Chen, Luminescence models, Radiat. Meas. 27 (1997) 625–661.
[56] V. Orante-Barrón, L. Oliveira, J. Kelly, E. Milliken, G. Denis, L. Jacobsohn, J. Puckette, E. Yukihara, Luminescence properties of MgO produced by solution combustion synthesis and doped with lanthanides and Li, J. Lumin. 131 (2011) 1058–1065.
[57] T. Yamashita, Y. Yasuno, M. Ikedo, Beryllium oxide doped with lithium or sodium for thermoluminescence dosimetry, Health Phys. 27 (1974) 201–206.
[58] N. Dhananjaya, H. Nagabhushana, B. Nagabhushana, B. Rudraswamy, C. Shivakumara, R. Chakradhar, Effect of Li+-ion on enhancement of photoluminescence in Gd_2O_3:Eu^{3+} nanophosphors prepared by combustion technique, J. Alloy. Compd. 509 (2011) 2368–2374.
[59] P. Dorenbos, A.J.J. Bos, Lanthanide level location and related thermoluminescence phenomena, Radiat. Meas. 43 (2008) 139–145.
[60] S.J. Dhoble, V.B. Pawade, H.C. Swart, V. Chopra, Spectroscopy of Lanthanide Doped Oxide Materials, Woodhead Publishing, 2019.
[61] G. Blasse, B. Grabmaier, A general introduction to luminescent materials, Luminescent Materials, Springer, 1994, pp. 1–9.
[62] V.S. Kortov, I.I. Milman, A.I. Slesarev, V.S. Kijko, New Beo ceramics for Tl Esr dosimetry, Radiat. Prot. Dosim. 47 (1993) 267–270.
[63] R. Balakrishnaiah, S.S. Yi, K. Jang, H.S. Lee, B.K. Moon, J.H. Jeong, Enhanced luminescence properties of YBO_3:Eu^{3+} phosphors by Li-doping, Mater. Res. Bull. 46 (2011) 621–626.
[64] V. Altunal, V. Guckan, A. Ozdemir, K. Kurt, A. Ekicibil, Z. Yegingil, Investigation of luminescence properties of BeO ceramics doped with metals for medical dosimetry, Opt. Mater. 108 (2020) 110436.
[65] A.M. Stoneham, Theory of Defects in Solids: Electronic Structure of Defects in Insulators and Semiconductors, Oxford University Press, 2001.
[66] P. Dorenbos, Systematic behaviour in trivalent lanthanide charge transfer energies, J. Phys. Condens. Matter 15 (2003) 8417–8434.